João Paulo Palma Jacinto

Licenciado em Ciências de Engenharia de Micro e Nanotecnologias

Nanocomposite Polymer Beads for Cell Detection

Dissertação para obtenção do Grau de Mestre em

Engenharia de Micro e Nanotecnologias

Orientadores: Doutor Carlos Rodríguez- Abreu, Staff Researcher, International Iberian Nanotechnology Laboratory

Co-orientador: Professor Doutor João Paulo Miranda Ribeiro Borges, Professor Auxiliar, Departamento das Ciências dos Materiais, Faculdade de Ciências e Tecnologias da Universidade Nova de Lisboa

FACULDADE DE CIÊNCIAS E TECNOLOGIA
UNIVERSIDADE NOVA DE LISBOA

Nanocomposite Polymer Beads for cell detection

Acknowledgments

I would like to thank to Carlos Rodríguez- Abreu for the opportunity to work in this project and also for all the help and guidance during my six months stay at INL.

Agradeço ao Professor João Paulo Borges, por ter aceite co-orientar este trabalho e por sempre se ter mostrado disponível em tudo o que foi necessário para que um bom trabalho fosse realizado.

I have to also thank to Ana Villa for helping me with the functionalization of the nanocomposite polymer beads and all the support during my stay.

Ao Professor Rodrigo Martins e à Professora Elvira Fortunato pela criação, desenvolvimento e promoção do curso de Engenharia de Micro e Nanotecnologias,

Manuel Bañobre and Juan Gallo, I could not be more grateful for the help with the XRD characterization and also for the aid with all the other techniques I was not able to perform by myself.

Um grande obrigado ao Alexandre Chícharo por ter tido a disponibilidade em ajudar-me com o COMSOL, e mais do que isso por ter arranjado tempo para me explicar grande parte do seu trabalho enquanto estudante de doutoramento.

Quero também agradecer a todos os que fizeram parte da minha estadia no INL nestes 6 meses. À Elizabete Fernandes por me ter ajudado quando precisei, com as conversas no café, quem sabe se ainda não te envio cogumelos da minha plantação.

Noelia e José obrigado pela companhia e pela ajuda no laboratório, pelas saídas e pelos jantares partilhados.

Yury Kolen'ko thank you for all the “How is Life?” questions, the amazing music in your laboratory and for all the laughs.

Haluan kiittää Lauraa kaikesta avusta laboratoriossa. Sitäkin enemmän olen kiitollinen yhteisille keskusteluillemme antamastasi ajasta, enkä voi kiittää sinua tarpeeksi kaikista neuvoista ja opastuksesta, joita sain sinulta näiden kuuden kuukauden aikana.

Um agradecimento mais que especial à Rita Peixoto, sem ti nestes 6 meses não tinha sido tão fácil. Todos os almoços, todas as boleias os cafés e acima de tudo a companhia que espero um dia conseguir retribuir.

Temo não ter espaço para conseguir agradecer a todos os que fizeram parte do meu percurso nestes últimos 5 anos. Aos habitantes do Basolho: Júlio, o melhor ainda está para vir, Marrocos e o Interrail foi só treino. Diogo Vaz ainda falta muito concerto hipster/underground para experienciar. Moisés Tereso, por todos os documentários super interessantes que pude ver na tua TV durante a minha estadia nesta casa.

Ao Daniel Pereira, Trofas agora renomeado Profas, obrigado por toda a ajuda a nível académico, mas muito mais que isso obrigado por toda a paciência e por sempre te teres preocupado mesmo quando não tinhas que o fazer.

Coelho, já todos te fizemos crer que o Porto é grande podes parar.

Farah please learn to speak Portuguese for once, I am now happy that you now know who the President of Portugal is, and that Lombarda is couve. Thank you, Aubergine.

Obrigado à Sofia Martins, Joana Almeida e à Constança Oliveira por terem feito parte das festas, dos jantares dos cafés e de tudo o que valeu a pena.

Sara obrigado por tudo o que fizeste, pela ajuda pela companhia e por sempre ter podido contar contigo independentemente da circunstância.

Jamie mesmo a 15 000km de distância continua a ser contigo que falo todos os dias, obrigado por teres ajudado no que podias e no que não podias.

Agradeço ao Diogo por ter estado presente em grande parte do percurso e me ter apoiado incondicionalmente.

Por fim e mais importante que tudo agradeço aos meus pais, à minha irmã e aos meus avós. Porque o esforço nunca foi só meu.

Abstract

Circulating tumor cells (CTCs) may induce metastases when detached from the primary tumor. The numbers of these cells in blood offers a valuable prognostic indication. Magnetoresistive sensing is an attractive option for CTC counting. In this technique, cells are labeled with nancomposite polymer beads that provide the magnetic signal. Bead properties such as size and magnetic content must be optimized in order to be used as a detection tool in a magnetoresistive platform. Another important component of the platform is the magnet required for proper sensing. Both components are addressed in this work. Nanocomposite polymer beads were produced by nano-emulsion and membrane emulsification. Formulations of the oil phase comprising a mixture of aromatic monomers and iron oxide were employed. The effect of emulsifier (surfactant) concentration on bead size was studied. Formulations of polydimethilsiloxane (PDMS) with different viscosities were also prepared with nano-emulsion method resulting in colloidal beads. Polycaprolactone (PCL) beads were also synthetized by the membrane emulsification method. The beads were characterized by different techiques such as dynamic light scattering (DLS), thermogravimetric analysis (TGA) and scanning electron microscopy (SEM). Additionally, the magnet dimensions of the platform designed to detect CTCs were optimized through a COMSOL multiphysics simulation.

Keywords: Circulating Tumor Cells, Nano-Emulsion, Membrane Emulsification, Solvent Evaporation, Nanocomposite Polymer Beads, Magnetoresistive platform

Resumo

Células tumorais em circulação (CTCs) possuem a capacidade de induzir metástases quando são libertadas do tumor primário. O número destas células no sangue oferece indicação valiosa do prognóstico. A detecção magnetoresistiva é uma opção atractiva para a contagem de CTCs. Nesta técnica, as células são marcadas com contas poliméricas nanocompósitas que garantem um sinal magnético. As propriedades das contas tais como, o tamanho e conteúdo magnético, têm que ser optimizadas de modo a poderem ser utilizadas como ferramenta de detecção numa plataforma magnetoresistiva. Outro componente importante da plataforma é o magnete necessário para detecção. Ambos os componentes são estudados neste trabalho. As contas poliméricas nanocompósitas foram produzidas por nano-emulsão e emulsão por membrana. Formulações da fase dispersa contendo uma mistura de monómeros aromáticos e óxido de ferro foram utlizados. O efeito da concentração do emulsificante (surfactante) no tamanho das contas foi estudado. Formulações de polidimetilsiloxano (PDMS) com diferentes viscosidades foram também preparadas com o método de nano-emulsão resultando em contas coloidais. Contas de policaprolactona (PCL) foram também sintetizadas pelo método de emulsificação de membrana. As contas foram caracterizadas por diversas técnicas tais como dispersão dinâmica de luz (DLS), analise termogravimétrica (TGA) e microscopia electrónica de varrimento (SEM). Adicionalmente, as dimensões do magnete da plataforma utilizada para detectar CTCs foram optimizadas através uma simulação com recurso ao software COMSOL multiphysics.

.

Palavras-chave: Células tumurais em circulação, Nano-Emulsão, Emulsão por membrana, Evaporação de solvente, Contas Poliméricas Nanocompósitas, Plataforma magnetoresistiva

Abbreviations

ADVN	2,2'-Azobis (2,4-dimethyl) valeronitrile
AIBN	Azobisisobutyronitrile
BSA	Bovine serum albumine
CTC	Circulating tumor cell
CD45	Cluster of differentiation 45
DLS	Dynamic light scattering
DVB	Divinylbenzene
EDC	1-Ethyl-3-(3-dimethylaminopropyl)carbodiimide
EpCAM	Epitelial cell adhesion molecule
FDA	Food and drug administration
MA	Methacrylic acid
MR- Biochip	Magnetoresistive biochip
MRI	Magnetic resonance image
MTJ	Magnetic tunnel junctions
O/W	Oil in water
PBS	Phosphate buffered saline
PCL	Polycraptolactone
PDMS	Polydimetilsiloxane
PI	Polydispersitity index
PIC	Phase Inversion Composition
PIT	Phase Inversion Temperature
Rpm	Rotations per minute
SDS	Sodium dodecyl sulfate
SEM	Scanning electron microscope
Styr	Styrene
SV	Spin-valve
TGA	Thermal gravimetric analysis
UV	Ultra-violet
W/O	Water in oil

Symbols

Å	Ångstrom
D	Diffusion coefficient
d_d	Droplet diameter
d_p	Pore diameter
E_B	Energy barrier
emu/g	Mass magnetization
Fe^{2+}	Ferrous iron
Fe^{3+}	Ferric iron
H	Magnetizing force
K_B	Boltzmann constant
M_s	Magnetization saturation
Mn	Average molar mass
Oe	Oersted
T	Temperature
t	Time
T_1	Longitudinal relaxation time
T_2	Transversal relaxation time
T_B	Blocking temperature
V_m	Molar Volume
wt%	Weight percentage
ΔA	Interfacial area variation
ΔG	Free energy variation
ΔS	Entropy variation
θ	Contact angle
γ	Interfacial tension
C_∞	Solubility of the dispersed phase in the continuous phase
ρ	Density

Table of Contents

List of Figures

List of Tables

Objective

Nanotechnology has enabled the production of tailored nanometric particles with functional uses for biomedical applications and diagnosis. The framework of this thesis aims to synthetize polymer beads with encapsulated magnetic nanoparticles. Diverse formulations of polymers are used for the synthesis to study how they affect performance. Two different techniques of synthesis are employed: mini-emulsion and membrane emulsification followed by solvent evaporation. The polymer beads synthetized are functionalized with antibodies in order to detect and quantify circulating tumor cells in blood samples through a magnetoresistive platform. Optimization of the magnet dimensions used in the platform is carried out through a COMSOL Multiphysics simulation.

Motivation

Metastatic cancer is incurable. Monitoring circulating tumor cells (CTCs) in blood has a prognostic value, and helps in the clinical management of cancer patients. However the detection of this specific type of cancer cells, which can induce metastasis, is a scientific challenge. This is so given the scarcity of the circulating tumor cells in peripheral blood, even in patients in an advanced cancer stage.[1]

The current commercial Food and Drug Administration (FDA) approved method to detect and quantify circulating tumor cells requires a highly qualified person. The enrichment of cells is immunomagnetic and there is a positive selection using EpCAM – labeled iron oxide nanoparticles, a subsequent detection of cytokeratin-positive CTCs is made. Cytomorpologic characteristics of tumor cells such as: size, presence of nucleus and appropriate nuclear to cytoplasmic ratio are accessed by scientific personnel. This step is the major source of error given the qualitative evaluation.It is expected that in the future a simple, inexpensive, automated method could be able to detect and quantify circulating tumor cells in peripheral blood in a hospital context[2][3].

In order to enable this vision, a broad spectrum of different scientific disciplines, such as physics, chemistry and biology are necessary. Recent research in the area of quantification and detection of circulating tumor cells show different approaches can be made to tackle the problem [4].

In this project the detection and quantification of CTCs is conducted by a magnetoresistive platform[5][6]. The labeling of the cells is done by functionalized nanocomposite polymer beads which are superparamagnetic, i.e. they do not show remanent magnetization. The polymeric beads are synthetized by different emulsion techniques and functionalized with antibodies such as EpCam. The functionalized beads are able to bind to the CTCs and detection in the magnetoresistive platform is then possible[7]

Chapter 1 – Introduction

1.1 - Overview on circulating tumor cells

Primary tumor cells spread to distant sites of the body through invasion into blood and lymphatic vessels. Hematological spread of cancer occurs when a circulating tumor cell (CTC) detaches from a primary tumor, enters the blood stream and eventually forms a new metastasis at a distant site. CTCs were first reported in peripheral circulation by Ashworth in 1869[8], this type of cells are usually larger than the constituents of blood, with an average diameter of 10.7µm in the case of prostate cancer, 11µm in colorectal cancer and 13.1µm in breast cancer. Human blood consists of white blood cells (5-10 10^6/ml), red blood cells (5-9 10^9/ml) and platelets (2.5-4 10^8/ml), there are very few CTCs present in blood even in patients with known metastatic disease, often less than one per ml of blood. [2,3]

Cancer patients undergoing treatment usually go through blood draws, and this is ideal for the detection of metastatic tumor cells, because it is easier, faster and less invasive than collecting a tissue biopsy. CTCs have a prognostic relevance and also predict response of patients to therapy [1].

Cristofanilli *et al.* established the threshold of 5 tumor cells/7.5ml of blood in order to define the prognostic significance of CTCs in breast cancer, the authors demonstrated that the changes in CTCs number predicted the response, or lack of it to the therapy [10]. This threshold level was later used in subsequent studies for prostate and colorectal cancers (the previous used a threshold of three tumor cells), which concluded that CTC detection was also associated with unfavorable outcome. [9]

1.1.1 Enrichment and detection of CTCs

As previously mentioned CTCs are very scarce in blood, therefore there is a need to enrich them prior to their detection. The techniques used for CTCs enrichment are based in the biological or physical properties that distinguish them from normal blood cells. A common used method for distinguish these cells is by affinity-based enrichment. This kind of approach uses distinctive antigens expressed by CTCs and not by blood cells, such as EpCAM, or by blood cells and not CTCs, like CD45. After enrichment, usually an immunomagnetic separation follows with magnetic beads functionalized with antibodies. In this approach, there can be a positive or negative enrichment, in the first case the antibodies of the functionalized bead bind to the CTC while in the second there is a binding to the blood cells. The major drawback of this approach is that not all tumor cells express the EpCAM antigen, e.g. renal cell cancer, and some others, e.g. breast cancer, express it heterogeneously. [1]

Circulating tumor cells have a difference in size when compared to blood cells. This property allows a physical approach to enrich the cells such as size-based separation, since CTCs are bigger. The main advantage of this technique is that a broad range of tumors are susceptible to this kind of separation and the heterogeneity of antigen expression is not and impediment to separation. This kind of approach is usually faster when compared with affinity-based separation techniques. [1][11]

In order to detect and enrich CTCs several methods have been proposed, such as microchip platforms, based in microfluidics which can be centered on size or affinity. [1]

However, a unique position has been achieved by CellSearch© System by Veridex/Johnson and Johnson (New Jersey, USA). It is the only validated method for detection of CTC and has undergone a preclinical and clinical validation. The immunomagnetic enrichment is based on positive selection using iron oxide nanoparticles labeled with EpCAM, and subsequent detection of cytokeratin-positive CTCs. The system also counts as a tumor cell the ones that express cytokeratins but do not express CD45, and that have the cytomorphologic characteristics of tumor cells [1]. The method provides a standardized and automated platform to detect tumor cells in the blood, the final classification of CTC is done by the operator and is the main contributor of the error of the assay. [2]

1.2 - Iron Oxide Nanoparticles – Magnetite

Nanotechnology has made possible the fabrication and characterization of functional nanoparticles for biomedical applications. Iron oxide nanoparticles have been investigated with particular interest, especially magnetite which has a proven biocompatibility and shows a superparamagnetic behavior in the nanometer size range. [12]

Magnetite, Fe_3O_4, is a magnetic iron oxide having a cubic inverse spinel structure with oxygen forming a fcc close packing and Fe cations occupying interstitial tetrahedral sites and octahedral sites, as shown in Figure 1[13]. The electrons can hop between Fe^{2+} and Fe^{3+} ions in the octahedral sites at room temperature which characterizes magnetite as a semi-metallic material. Magnetite nanoparticles can be dispersed in various solvents and form homogeneous suspensions if the nanoparticle´s surface is properly coated. [14]

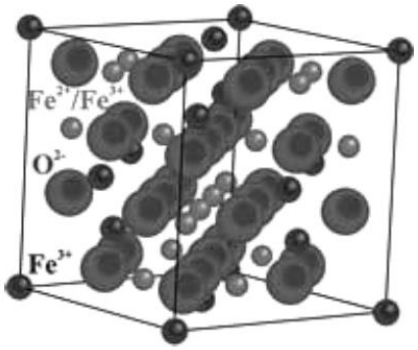

Figure 1– Structure and unit cell of magnetite [9]

The saturation magnetization values found in nanostructured materials are usually smaller than the corresponding bulk phases. Accordingly, experimental values for M_S in magnetite nanoparticles vary in the range 30-50 emu/g, values that are lower than the bulk magnetite value of 90emu/g. This occurs because of the spin disorder effects at the surface of the nanoparticles[15].

1.2.1 –Superparamagnetism

Superparamagnetism is a size-related magnetic behavior exhibited in single domain particles [16]. As the particle size is reduced the domain walls cease to exist and particles show only a single magnetic domain instead of multi-domain. Superparamagnetic particles have magnetic anisotropy, spins align in a preferred orientation and therefore it is easier to align them in that direction. The anisotropy can derive from size, shape or stress. In order to overcome the anisotropy there is a need to provide thermal energy. The thermal activation over the magnetic anisotropy energy is described by equation 1.

$$f = f_0 exp(-E_b/kT) \quad (1)$$

where f_o, is the attempt frequency, kT is the Boltzmann term and E_b the energy barrier[17]. The blocking of superparamagnetic particles occurs bellow the blocking temperatureT_B. Below this temperature particles have coercitivity and remanence. A hysteresis curve with coercitivity exists below the blocking temperature as seen in Figure 2a). In contrast, above T_B, there is no coercitivity and the curve intersects the origin of coordinates, as shown in Figure 2b). Unless a magnetic field is applied, the superparamagnetic material will show paramagnetic characteristics; otherwise the spins align along the line of easy magnetization. [18].

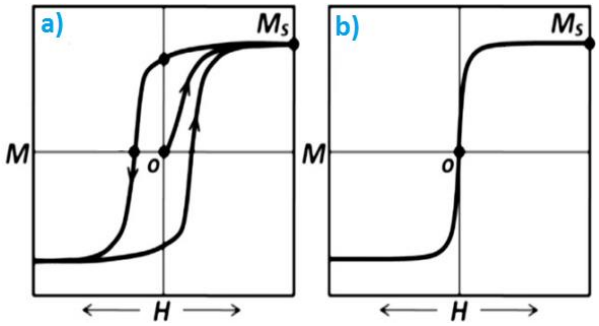

Figure 2 – Illustration of a typical hysteresis loop a), and typical curve of superparamagnetic material b), adapted from [18] ***. M, M_s and H are the magnetization, the saturation magnetization and the magnetic field strength.***

1.2.2 – Synthesis of iron oxide magnetic nanoparticles

There are essentially two means of synthetizing iron oxide nanoparticles: physical methods, such as phase deposition and electron beam lithography, or wet chemical routes. The physical methods generally do not allow to control the size of the particles therefore the chemical approach is preferred, since it is possible to tune size, shape and composition[14]. This is achieved by controlling the type of salts used, Fe^{2+} and Fe^{3+} ratio, pH and ionic strength of the reaction media[19].

Magnetite can be prepared by adding a base to an aqueous mixture of Fe^{2+} and Fe^{3+} chloride at a 1:2 molar ratio[20]. The chemical reaction is written as:

$$Fe^{2+} + 2Fe^{3+} + 8OH^- \rightarrow Fe_3O_4 + 4H_2O \quad (2)$$

Complete precipitation of magnetite is expected between, pH 9 and 14, while the molar ratio is the one mentioned above under a non-oxidizing, oxygen-free environment. Otherwise, magnetite can be oxidized according to:

$$Fe_3O_4 + 0.25O_2 + 4.5H_2O \rightarrow 3Fe(OH)_3 \quad (3)$$

This alters the physical and chemical properties of the particles[13]. Therefore, in order this to be prevented, during precipitation nanoparticles should be coated. An oxygen-free atmosphere, with the use of N_2, not only ensures protection from oxidation but also favors smaller particle sizes [21].

During the synthesis of nanosized magnetite, larger particles begin to grow at the expense of the smaller ones, because it is more favorable to have atoms in the bulk than on the surface, therefore bigger particles tend to grow bigger. This mechanism of growth is called Ostwald ripening, as depicted in Figure 3 [22].

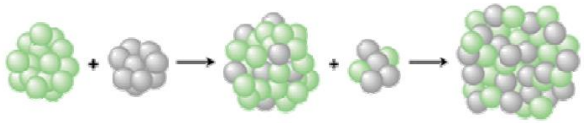

Figure 3 – Ostwald ripening: to decrease surface energy, larger particles grow at the expense of the smaller ones. [18]

1.3.1 – Nano-emulsions

An emulsion is a system containing two immiscible phases, where one is the dispersed or internal phase in the form of droplets, and the other is the continuous or external phase[23]. Emulsions can be categorized in two types: water-in-oil, W/O, also named inverse emulsion, and oil-in-water, O/W, named direct emulsion. This categorization depends on whether the phase dispersed in droplets is hydrophilic, polar, or hydrophobic, non-polar, respectively [24]. In order to create an emulsion there is a need to apply shear, this will cause the droplets of one phase to stretch and rupture into smaller droplets [25]. An emulsion with a droplet size between 20-200nm is called nano-emulsion [26].

The components needed to prepare an emulsion are oil, water, surfactant and energy. Equation 4 enables the calculation of the total free energy of formation of an emulsion (ΔG).

$$\Delta G = \gamma \Delta A + T \Delta S \quad (4)$$

Where ΔA, is the change in specific in interfacial area, γ, is the interfacial tension, T, is the temperature of the process and ΔS the entropy change. Accordingly, a decrease in specific in interfacial area (negative ΔA) is an spontaneous process (negative ΔG); emulsions are therefore thermodynamically unstable systems as negative ΔA implies droplet disruption towards phase separation [27].

Nano-emulsions, being non-equilibrium systems, need energy to be formed; this can be obtained from a mechanical device or from the chemical potential of the components. Therefore preparation of nano-emulsions can be categorized in high energy methods and low energy methods. High energy methods include high-shear stirring, high-pressure homogenizers and ultrasound generators. Low energy methods take advantage of physicochemical properties of the system such as the method of phase inversion temperature, PIT, phase inversion composition, PIC, and solvent diffusion [28][29].

1.3.2 - Ultrasonic emulsification

Within the ultrasound range the power varies inversely with the frequency, and only very powerful ultrasounds, 16-100 kHz, can interact with matter, producing physical and chemical changes essential by cavitation phenomena[30].

Cavitation is the phenomenon responsible for ultrasonically induced effects. Acoustic cavitation associated with power dissipation, is the driving force in sonochemical processing, and is the essential mechanism of droplet breakup occurring during ultrasound emulsification[31]. In figure 4 a scheme of the cavitation process is described. The cavitation bubbles originate from nuclei, eg. preexistence microbubbles in the bulk of the liquid. They act as hotspots where high pressures and temperatures are reached [30].

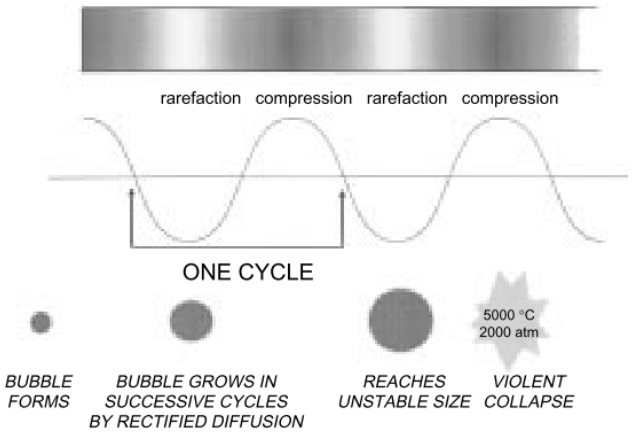

.

Figure 4 – Sound propagation in a liquid, cavitation bubble formation and collapse. [26]

Acoustic cavitation is as Ashokkumar quoted: “growth and collapse of micro-bubbles under and ultrasonic field”[32].

In order to create an emulsion using ultrasound it is needed energy. The energy that is required by continuous phase in the form of shear to break droplets of dispersed phase is expressed in terms of Laplace pressure,p, equation 5. Laplace pressure is the difference in pressure between outside and inside of the droplet.

$$p = \gamma \left[\frac{1}{R_1} + \frac{1}{R_2}\right] = \frac{\gamma}{2R} \tag{5}$$

R_1 and R_2 are the radius of curvature of perfectly spherical droplets, so $R_1 = R_2$, and γ is the interfacial tension of droplets. Emulsions are created when the pressure due to applied shear stress is greater than the characteristic Laplace pressure, nano-emulsions require extremely high shear stress[33][25].

Optimization of ultrasound emulsification requires the controlling of ultrasonication parameters which are: energy, intensity, temperature and pressure. There is also a need to pay attention to the formulation variables such as: medium viscosity, surface tension and dissolved gas. All these parameters should be controlled in order to obtain stable nano-emulsions with fine droplets size and low polydispersity index.[34]

1.3.3 – Ostwald ripening mechanism in nano-emulsions

The primary mechanism that affects nano-emulsions and disrupts them is Ostwald ripening. In this process the smaller droplets, as a result of their higher chemical potential, dissolve and the material diffuses towards the larger drops [35].

The dispersed phase migrates through the bulk from the smaller droplets to the bigger ones, due to the higher solubility in the bulk of the smaller droplets. The rate in which this occurs depends on the solubility of the dispersed phase in the bulk phase and on the interfacial tension between the two phases, as predicted by Lifshitz, Slezov and Wagner theory of Ostwald ripening[36]. The rate of Ostwald ripening can be estimated from:

$$\omega = \frac{dr^3}{dt} = \frac{C_\infty \gamma V_m D}{\rho RT} \tag{6}$$

where C_∞, is the solubility of the dispersed phase in the continuous phase. D, is the diffusion coefficient. ρ and V_m, are the density and molar volume of the dispersed phase, respectively. R is the gas constant, T is the temperature and γ the interfacial tension of the droplets. The ripening rate should be low in order to have a stable nano-emulsion. This is normally achieved by decreasing the solubility of the dispersed phase in the continuous phase[24]. Ostwald ripening rate follows and Arrhenius law[37].

1.3.4 – Nano-emulsion polymerization

In nanoemulsion polymerization, also referrered as miniemulsion polymerization, the nano-emulsions are composed of pure monomer droplets surrounded by the adsorbed stabilizing surfactants. The prevalent way of inducing polymerization is by the addition of initiator molecules[27]. However it can also be UV-induced[38], ultrasonically induced[39] or even enzyme induced[39].

The accepted mechanism in which nano-emulsion polymerization occurs is described as droplet nucleation mechanism. It suggests the entrance of radicals in each one of the monomer droplets, and therefore these are taken as individual reaction sites. Having this in consideration one assumes that the particle number and size do not change during polymerization, and this is consistent with the trend that correlates the use of an oil-soluble initiator to the improvement of the number of nucleated droplets[40].

The previously mentioned initiator molecules, e.g. Azobisisobutyronitrile (AIBN), can be added to the initial nano-emulsion droplets, and then polymerization is triggered by raising the temperature of the system[41].

1.3.5 – Membrane Emulsification

Membrane emulsification is an attractive method to produce emulsions. In this process pressure is used to force the dispersed phase through a membrane, with a uniform pore-size distribution, into the continuous phase. This procedure enables the user to control the droplet size primarily by the choice of the membrane. It is a simple technique and results in narrow droplet size distributions, being applicable in both oil-in-water and water-in-oil emulsions, the process is illustrated in Figure 5.[42]

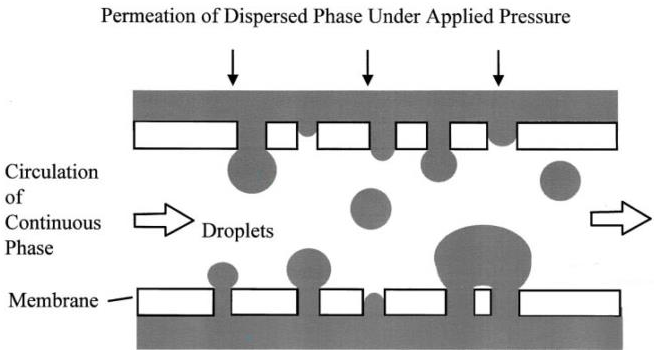

Figure 5 – Membrane emulsification process, adapted from [42]

Droplets will grow at the pores outlets until detachment. This is ruled by: drag force on the droplet from the circulating continuous phase, buoyancy of the droplet, the interfacial tension and the pressure applied to the system. The final droplet size and distribution is determined by the pore size and pore distribution in the membrane but also the degree of coalescence, at the membrane surface and in the bulk solution. [43]

There is a critical pressure at which the dispersed phase must be in order to permeate through the membrane, and it can be estimated as:

$$P_c = \frac{4\gamma cos\theta}{d_p} \quad (7)$$

where d_p is the pore diameter, γ is the interfacial tension and θ the contact angle between the dispersed phase and membrane surface. [44]

The droplet size is related to the pore size of the membrane by a linear relationship for given process conditions:

$$d_d = c\, d_p \quad (8)$$

where values of c range typically from 2 to 8, being c the constant between d_d, droplet diameter and d_p, pore diameter.[44]

As a rule the dispersed phase should not wet the membrane pores. Therefore the hydrophilic membranes are suitable to produce oil in water emulsions and the hydrophobic membranes for water in oil. The coalescence of the droplets is mainly due to the distribution of the pores, which means that the coalescence is most likely to occur if the pores are too close to each other (see Figure 5) [42].

1.4 – Magnetoresistive chip cytometer

Magnetoresistive sensors are micro-fabricated, can be integrated within microfluidic channels and can detect magnetically labelled cells. At the present it is possible to detect single micrometer size magnetic beads moving up to 23 mms^{-1} velocities through microfluidic channels using magnetoresistive sensors integrated on the channel bottom [45]. With this approach it is possible to isolate target cells directly from crude samples such as blood. [5]

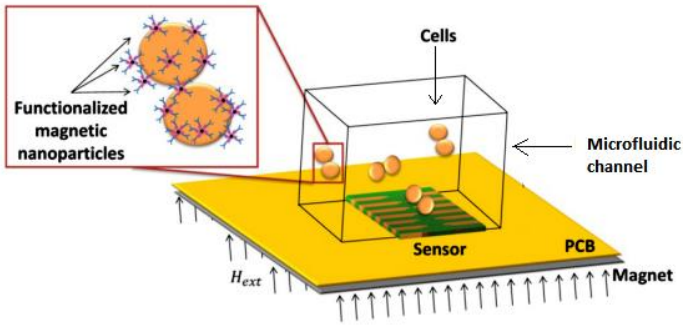

Figure 6- Typical Magnetoresistive device, adapted from [46]

Five main components can be identified in MR-biochip: the MR sensing elements, the magnetic labels, surface chemistry, microfluidic system and the electronic setup. The sensing elements are of two types: spin valves (SV) and magnetic tunnel junctions (MTJ). The magnetic labels used are magnetic nanoparticles which should be superparamagnetic, uniform in size and shape, and also have the right coating and functional surface modification. The surface

chemistry has to be controlled, therefore, the choice of the surface material is of extreme importance, and this can be gold or silica and depends of the purpose of the chip. Regarding microfluidics it is important that the polymers used are biocompatible, e.g.PDMS. In Figure 6 a typical magnetoresisitive device scheme is presented. The electronic setup must fulfill the following conditions: perform real-time signal processing, use standard technologies to shorten the development time, transmit and encrypt the data , and have a graphical user interface.[6]

Chapter 2 – Experimental and characterization techniques

2.1 – Synthesis, characterization and functionalization of nanocomposites polymer beads

Polymer beads with magnetite nanoparticles were prepared by mini-emulsion polymerization. Emulsions contained 10 wt% organic phase, which comprised a mixture of monomers Styrene (Styr), Divinylbenzene (DVB), Methacrylic acid (MA), all from Sigma Aldrich, and the initiator of polymerization 2,2'-Azobis (2,4-dimethyl) valeronitrile, (ADVN) obtained from DuPont.(Mass ratio Styr:DVB:MA:ADVN = 76:13:10:1). Octadecene (Sigma-Aldrich) was also used at 1 wt% in the organic phase in some emulsion formulations. A batch of magnetic oleic-acid-capped nanoparticles in cyclohexane synthesized by co-precipitation[14] (nanoparticle concentration = 64g/L size between 10-12nm) was used in all experiments.

The iron oxide nanoparticles were dispersed in the organic phase using an ultrasound bath (1 min). The emulsification was carried out in an aqueous medium of sodium dodecyl sulfate (SDS) (Sigma Aldrich) at various concentrations (0.1, 0.2, 1 and 2 wt%). The mini-emulsion was mixed through a VWR VDI 12 mixer at intensity 4 during 1 min, and then sonicated using a Fisher scientific CV 188 Vibracell equipment, at 60% amplitude for 1 min. Polymerization was then conducted at 60ºC under agitation (scale = 240) during 24h in a VWR incubating orbital shaker.

The same preparation methodology was also followed for an organic phase comprising polydimethylsiloxane (PDMS, ABCR), the cross-linker trimethylsilyl-terminated poly-(dimethylsiloxane-co-methyl hydrosiloxane) (Sigma-Aldrich) and the crosslinking catalyst platinum (0)-1,3-divinyl-1,1,3,3-tetramethyl-disiloxane (Sigma-Aldrich), The emulsions were prepared with and without the sonication step. Different concentrations of platinum catalyst in chloroform (1% , 3% and 9%), were used.

Magnetic polymer beads were also prepared by membrane emulsion technique. In this case an external pressure type micro kit from SPG Technology Co.,LTD was used. Different pore size hydrophilic membranes from SPG were also employed. The organic phase, the same used in mini-emulsion polymerization, was dispersed in two solvents: dichloromethane (Fischer Chemical) and hexane (Panreac). The continuous phase used was an aqueous medium of sodium dodecyl sulfate (SDS, 1 wt %). A continuous flow of compressed air was supplied to the bottom of the micro kit in order to help the detachment of the droplets during the emulsification process. The pressure of the module is manually increased until the critical pressure is reached and droplet detachment occurs. Evaporation of the solvent and polymerization of the beads were conducted at 60ºC for 24h.

Beads were also prepared using polycaprolactone (PCL $\overline{Mn}$ = 80 000) (Sigma Aldrich) For that , PCL was dissolved in chloroform, and the mixture was emulsified by membrane emulsification technique in an aqueous medium of sodium dodecyl sulfate (SDS, 1 wt %), following the procedure mentioned above. To obtain the beads, chloroform was evaporated at 50ºC.

Functionalization of the polymeric beads was conducted with the following method: to a batch of beads a maximum of 0.05% volume ratio of Tween ® 20, Sigma Aldrich is added. In order to activate the carboxylic groups of the polymer beads, an aqueous solution of 1-Ethyl-3-(3-dimethylaminopropyl)carbodiimide, EDC,Thermo Scientific) is used.

N-Hydroxysulfosuccinimide sodium salt (Sulfo – NHS, Thermo Scientific), a chemical modification reagent for converting carboxyl groups to amine reactive NHS ester is added and the mixture is incubated 15 min at room temperature with rotary stirring. Then the mixture is centrifuged at 10,000 rpm during 10 min. The supernatant is then removed. The precipitated solid is resuspended with Protein A solution in PBS in order to form amide bonds. Then the mixture is incubated 3h at 4ºC and centrifuged at 10,000 during 10 min. The supernatant is eliminated and the pellet resuspended in PBS 2%, BSA and Cell Staining Buffer 50:50. The product was stored at 4ºC.

The iron oxide particles were characterized by a diffractometer system XPERT-PRO with an anode material of Cu, $K\alpha_1$ and $K\alpha_2$wavelength of 1.541Å and 1.544Å respectively.

The size and polydispersity of the nanocomposite beads was accessed through Dynamic Light Scattering using a Horiba scientific SZ-100 and confirmed by scanning electron microscopy using a FEI Quanta ESEM.

The magnetic content was determined by thermogravimetric analysis (TGA) using a Mettler-Toledo TGA/DSC1 STARe system. Conditions for TGA scans are shown in Tables 1 and 2

Table 1- *Thermogravimetric analysis for dry samples*

Temperature	time	Atmosphere
25-800°C	20.00k/min	Ar 30.0ml/min
800ºC	5min	O_2 30.0ml/min

Table 2 - *Thermogravimetric analysis for wet samples*

Temperature	time	Atmosphere
25-100ºC	5.00k/min	Ar 30.0ml/min
100ºC	10min	Ar 30.0ml/min
100-800ºC	20.00k/min	Ar 30.0ml/min

2.2 – Optimization of the magnetoresistive platform

The reading of the magnetic field of a Q-40-20-05-Block magnet with 40 x 20 x 5 mm dimensions of Neodymium grade N42, nickel-plated magnet, acquired from Webcraft GmbH, was performed with a DSP Gaussmeter 455 and a Lake shore HMNT-4E04-VR probe with the magnet on a Thorlabs – Model L490MZM platform. The software used was created by Marco Martins at INL.

Several readings of parallel planes at different distances to the magnetized surface of the magnet were performed, with the purpose of comparison with the simulation, in order to validate the model used. Simulation was made using COMSOL Multiphysics software.

The microfluidic channel is at a 2.4mm distance from the magnet. The magnetic field that impinges the previously mentioned channel must have a maximum contribution in vertical direction Hz, and minimum contribution, close to zero in the horizontal axis. This will prevent aggregation of the magnetic beads and therefore have a positive impact in the signal given by the system.

Chapter 3 – Results and discussion

3.1 - Iron oxide nanoparticles

The diffraction pattern obtained from a sample of iron oxide nanoparticles is shown in figure 7. Several high intensity peaks are present, and are listed in Table 3. The data points to existence of magnetite [47] , however peak 7 is correspondent to maghemite. most likely the sample is a mixture of the two iron oxides since it is of extreme difficulty to prevent the oxidation of magnetite during the synthesis .[48][49]

Table 3- Identifiable peaks of iron oxide employed

No.	h	K	l	d [Å]	2Theta [°]	I [%]	Characteristic Peak[49]
1	0	2	2	2.9451	30.324	33.7	Fe_3O_4
2	1	1	3	2.51159	35.721	100	Fe_3O_4
3	0	0	4	2.0825	43.418	18.5	Fe_3O_4
4	2	2	4	1.70035	53.876	11.2	Fe_3O_4
5	1	1	5	1.60311	57.437	21.3	Fe_3O_4
6	0	4	4	1.47255	63.082	42.6	Fe_3O_4
7	3	3	5	1.27031	74.657	8.4	$\gamma - Fe_2O_3$

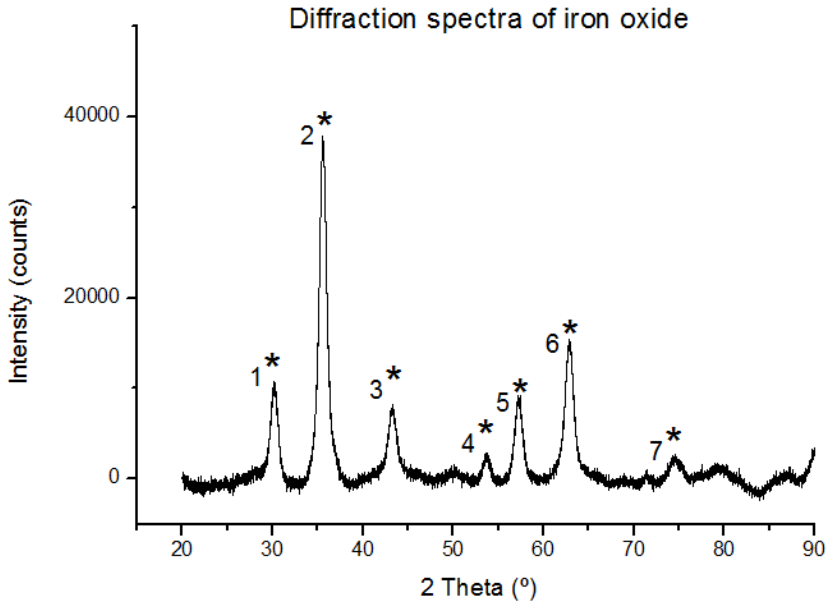

Figure 7 – Diffraction spectra of iron oxide nanoparticles employed with peaks identified

The peak broadening in the XRD spectra shown in figure 7 is related with the domain size of the crystals measured and also a possibility of lattice distortion due to different concentration gradients or dislocations in the crystal. [50]

3.2 – Nanocomposite polymer beads

3.2.1 Effect of the hydrophobic additive octadecene on polystyrene beads

Nanocomposite polymer beads were prepared using formulations with compositions shown in Table 4. The synthesized beads where characterized in terms of particle size by DLS, and in terms of iron oxide content by TGA. Characterization data are presented in Table 5

Table 4- Emulsion formulations with different contents of octadecene

	Oil phase						Aqueous phase
Sample	**Styr (g)**	**DVB (g)**	**MA (g)**	**ADVN (g)**	**Iron Oxide nanoparticles (g)**	**1-Octadecene (g)**	**SDS**
A	0.228	0.039	0.03	0.003	0.09	0	1%
B	0.228	0.039	0.03	0.003	0.09	0.003	1%
C	0.228	0.039	0.03	0.003	0.12	0	1%
D	0.228	0.039	0.03	0.003	0.12	0.003	1%

Table 5- Characteristics of bead synthesized from formulations in Table 4

Sample	**Theoretical iron oxide content**	**Size (nm)**		**TGA (%)**
		DLS		**Iron Oxide Content**
		Mean	**PI**	
A	30	96.5	0.4	19.1%
B	30	195.7	0.3	16.2%
C	40	174.0	0.3	24.1%
D	40	201.8	0.3	20.2%

As it is shown in table 5 the formulations that contained 1-octadecene are bigger in size, 100nm between samples A and B and 30nm between samples C and D. TGA data show that the iron oxide content is lower in samples with 1 – octadecene, 2.9% between the first two samples and 3.9% between C and D.

3.2.2 Effect of surfactant concentration on polystyrene beads

The effect of SDS concentration on particle size was studied using different emulsion formulations as shown in Table 6

Table 6 - Formulations with different concentrations of SDS

	Oil phase					Aqueous phase
Sample	Styr (g)	DVB (g)	MA (g)	ADVN (g)	Iron Oxide nanoparticles (g)	SDS
E	0.228	0.039	0.03	0.003	0.03	2%
F	0.228	0.039	0.03	0.003	0.03	1%
G	0.228	0.039	0.03	0.003	0.03	0.2%
H	0.228	0.039	0.03	0.003	0.03	0.1%

According to figure 8 there is a direct relationship between the concentration of surfactant SDS and the size of nanocomposites polymer beads obtained.

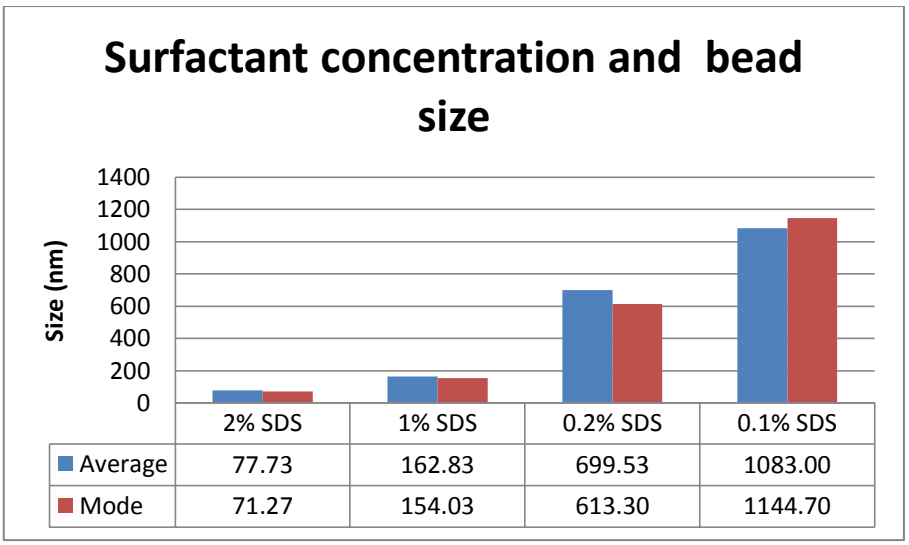

Figure 8 – Surfactant concentration and bead size, sample E to H

The size of the nanocomposite polymer beads follows and inverse relationship with the concentration of surfactant. Therefore it is possible to achieve smaller sizes if the concentration of surfactant is bigger. This is result is coherent with the scientific literature.[51]. However it is necessary to take in consideration the fact that as it is possible to observe in figure 9, the polydispersity index, PI, also increases when lower surfactant concentrations are used, this occurs because the low surfactant concentration is not enough to cover a large surface area of the future bead , therefore flocculation can happen resulting in an higher dispersity of sizes [52]. A SEM picture of sample G is shown in figure 10. This is an indication that there is a tradeoff between size and polydispersity. It is then necessary to take in account the final use of the nanocomposite polymer beads and if homogeneous size is essential.

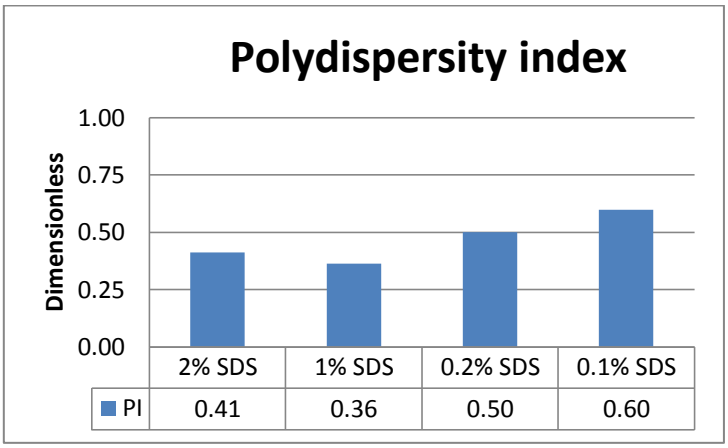

Figure 9 - Polydispersity index of samples E to H

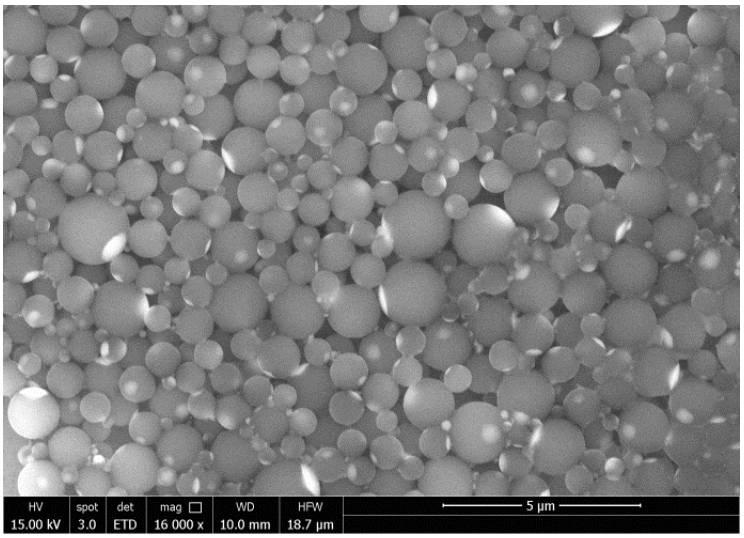

Figure 10 - SEM image of sample G

3.2.3 PDMS beads

PDMS nanocomposite polymer beads were also synthetized. The formulations used in the synthesis are listed in Table 7.

Table 7- Formulations used for the preparation of PDMS beads

		Oil phase					Aqueous phase
	PDMS (g)	**PDMS viscosity (cSt)**	**Crosslinker(g)**	**MA (g)**	**Pt Catalyst[1] (g)**	**Iron Oxide nanoparticles (g)**	**SDS**
	0.179	0.7	0.121	0.03	0.015	0.03	1%
	0.179	4-8	0.121	0.03	0.015	0.03	1%
	0.179	100	0.121	0.03	0.015	0.03	1%

[1] From a previously prepared solution of 9% Pt catalyst in chloroform

Stable emulsions were obtained when using PDMS as the dispersed (oil) phase. There was no considerable effect of PDMS viscosity on the particle size as seen in figure 11.

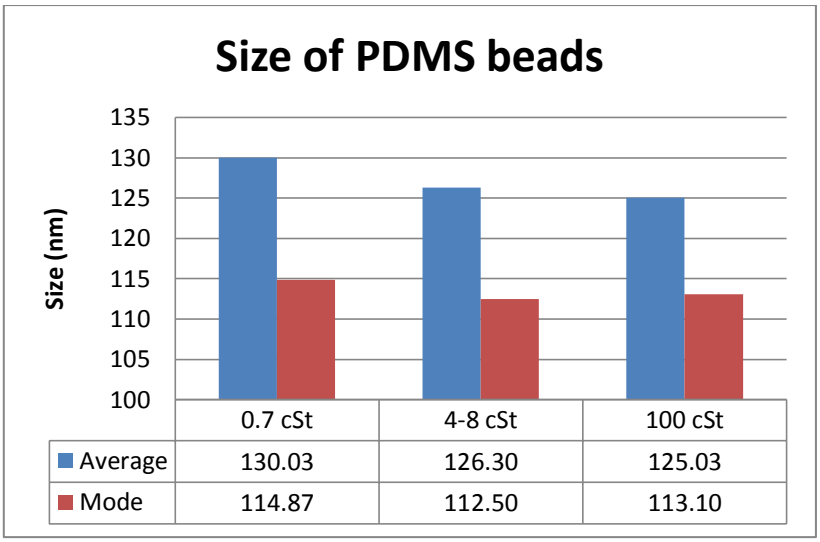

Figure 11- PDMS beads size

Figure 12 shows a SEM image of beads synthetized using 100cSt PDMS. The beads are spherical and polydisperse.

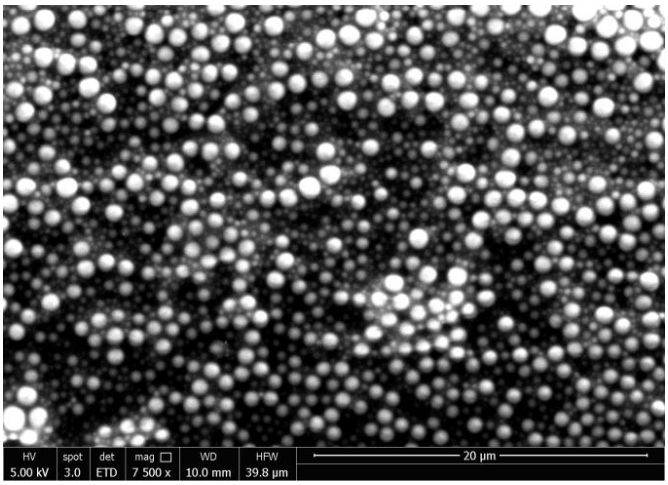

Figure 12 – SEM image of PDMS nanocomposite beads with 100cSt viscosity as starting material

3.2.4 Membrane emulsification

With the aim of obtaining a narrower size distribution, membrane emulsification followed by solvent evaporation was conducted. Two polymers were tested, polystyrene and polycraptolactone. The formulations used in the synthesis of polystyrene beads are shown in Table 8; the preparation conditions are shown in Table 9. The formulations used in the synthesis of polycaprolactone beads are shown in Table 10.

Table 8- Formulation for membrane emulsification to obtain polystyrene beads

	Oil phase				Solvent		Aqueous phase
Sample	Styrene (ml)	DVB (ml)	MA (ml)	ADVN (g)	DCM (ml)	Hexane (ml)	SDS
MA	0.24	0.04	0.03	0.003		2.1875	1%
MB	0.24	0.04	0.03	0.003	2.1875		1%
MC	0.24	0.04	0.03	0.003		2.1875	1%
MD	0.24	0.04	0.03	0.003	2.1875		1%

Table 9- Membrane pore size employed and pressure at which emulsification occurs

Sample	Membrane Pore size (µm)	Pressure (kPa)
MA	0.6	105
MB	0.6	65
MC	0.8	30
MD	0.8	55

Table 10- Formulation for membrane emulsification to obtain polycaprolactone beads

	Oil phase	Solvent	Aqueous phase	
Sample	PCL 80 000 (g)	Chloroform(ml)	SDS	Iron oxide nanoparticles (g)
MPCL1	0.21g	3	1%	0
MPCL2	0.21g	3	1%	0.02g

Table 11 - Membrane pore size employed and pressure at which emulsification occurs

Sample	Membrane Pore size (µm)	Pressure (kPa)
MPCL1	0.6	385
MPCL2	0.8	225

The samples MA, MB, and MC when measured in DLS showed a bimodal size distribution which was an indication of two size populations, and therefore a polydispersity index that was not suitable for application. This most likely happened due to the constant changing in

the supply air flow while achieving the critical pressure needed. The results do not suggest a difference in the different solvents used and the size of the nanocomposite beads obtained.

When the mentioned problems were perceived, 500 nm polystyrene beads were obtained through membrane emulsification sample MD, with a very low polydispersity index as it is shown in table 12.

Table 12 - DLS data of sample MD

Sample	Mean	Mode	PI
MD	506.97	503.30	0.19

Table 13 – DLS data of sample PCL samples

Sample	Mean	Mode	PI
MPCL1	1146.47	1137.53	0.66
MPCL2	1521.13	1515.97	0.57

Regarding PCL due to the viscosity of the starting components there was a necessity to only use a 7% solution (0.21g of PCL in chloroform) instead of 8%. This was enough to achieve the membrane emulsification process; however it was not possible to synthetize beads with size less than one micron. Nevertheless it was possible to make the synthesis with iron oxide in the oil phase, in table 13 DLS data for MPCL1 and MPCL2 samples is shown.

3.3 – Optimization of magnetoresistive platform

Eleven different simulations and readings of the vertical component magnetic field,Hz, at different planes were conducted and results shown in annex 1. The plane zero corresponds to a 0.1mm distance above the magnet. The subsequent planes correspond to the number of millimeters added to plane zero. Therefore plane 1 corresponds to 1.1mm and plane 2 to 2.1mm and so forth.

As it is shown in the first two simulations namely 0 and 1, the different intensity areas of the simulation and the reading match each other. The simulated magnetic field is however of poor accuracy at high intensity fields. This is due to computation limitations regarding the different mesh sizes used.

Differences between the read and the simulated values of the considered planes can be due to various factors. During the reading, there is no fine control of the alignment of the magnet or the probe, consequently this manual alignment may affect the results obtained. There is also a need to consider that the detector which does the reading, inside the probe is not at the very tip of the device, therefore intensity readings may be affected. Something that is important to have in consideration is the inhomogeneity of the magnet used. This is shown in reading planes 2, 3 and 6 where several high intensity spots appear. In readings 4, 5, 6 and 7 it is possible to perceive that isomagnetic lines in Hz are also not homogeneous.

Something that also needs to be taken in consideration is the fact that between the simulated and reading planes there is a considerable difference among the negative values

measured. In the simulated magnet the negative part of the magnetic field appears in plane 3 and is always present in the subsequent ones. In comparison in the actual reading a negative component in Hz is never present. This is due to the finite air box that needs to be simulated whereas in the actual reading this is infinite.

The conducted comparison offers a certain confidence in the results obtained in figure 13 and 14. Here it was studied the higher value of the vertical component of the magnetic field for different dimensions and thickness figure 13. The available distance without a horizontal magnetic component is presented in figure 14.

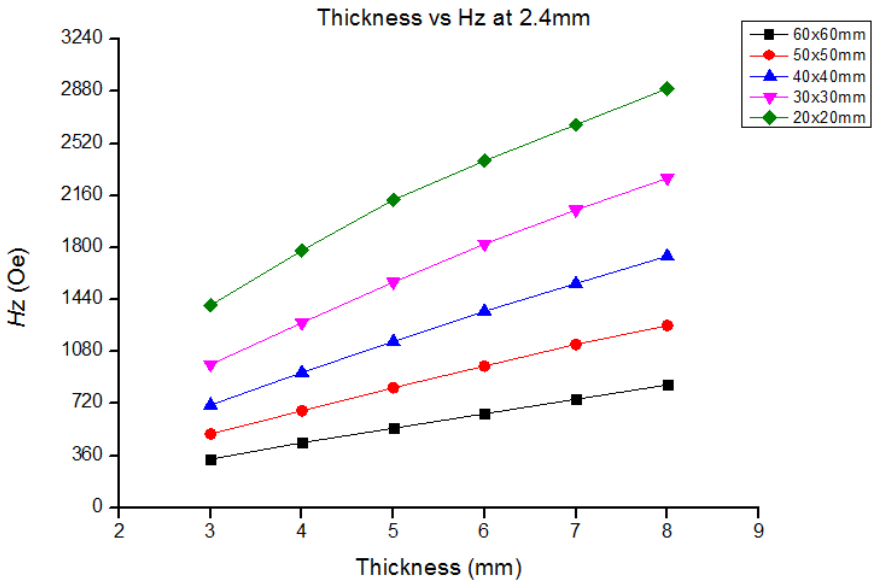

Figure 13 – Thickness of the magnet versus Hz at the center of the magnet

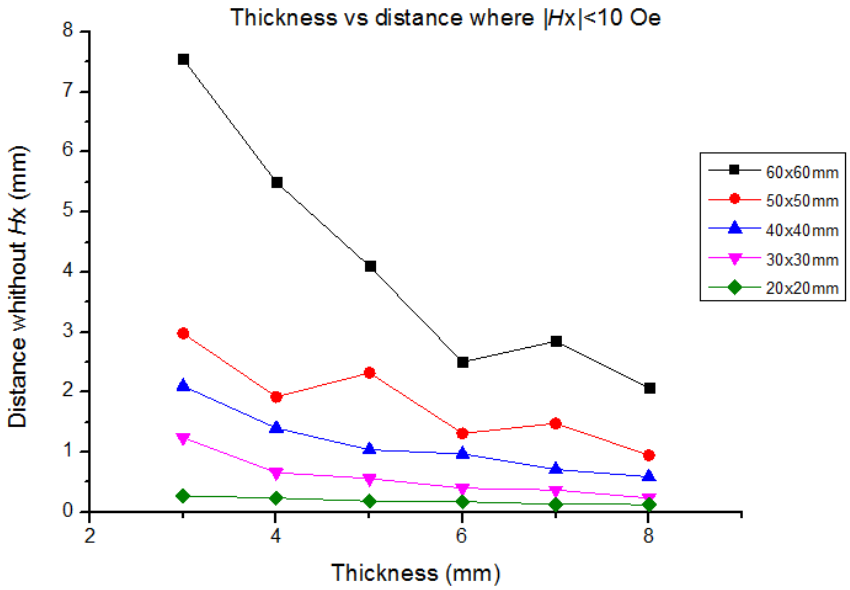

Figure 14 – Thickness of the magnet versus distance without Hx

A minimum of approximately $Hz = 1000\,Oe$ and a maximum available area with minimized Hx ($|Hx|$< 10 Oe) component. This conditions are required for a suitable magnetization of the beads in z direction thus ensuring a larger transduced signal by the magnetoresistive sensors. Secondly a minimized Hx is required to prevent saturation of the sensor linear range response.

Given this conditions, the ideal magnet would be very thick in order to provide a large value of Hz and the magnetized surface should have a very vast area. However this would make a bulkier and heavier device which is not aligned with the requisites of a point of care (POC) device. A compromise between magnet dimensions and requirements of a POC should be attained. A likely choice for the magnet can be the 30x30x3 mm magnet which provides $Hz = 990$ and a distance of 1.24mm with $|Hx| < 10\,Oe$ horizontal magnetic field component, which translates to 1.54 mm^2 of working area for the microfluidic channel.

Chapter 4 – Conclusion and future perspectives

Nano-emulsion is a versatile method which enables the production of nanocomposite polymer beads. It is possible to tune the size and the iron oxide content according to necessity. There are different ways to adjust the size of the beads. One of the possibilities addressed was accomplished by changing the surfactant concentration in the aqueous phase from 2% to 0.1%. This approach showed promising results as beads were obtained with size ranging from 70nm to 1µm with 10% theoretical iron oxide content dispersed in the polystyrene matrix.

The synthesis of PDMS nanocomposite polymer beads through nano-emulsion, with different starting PDMS viscosities, was successfully realized. Nanocomposite polymer beads with sizes ranging from 125nm (PDMS 100cSt), to 230nm (PDMS 0.7cSt), were obtained. An attempt was made to synthetize PDMS nanocomposite polymer beads using only the ultra-turrax avoiding the sonication step. However this was not possible to perform, the final solution was not stable and no final product could be retrieved. This shows that the sonication step is of vital importance in the process.

A problem that prevailed while using the nano-emulsion method was the polydispersity that is inherent to the technique. In order to overcome this problem, membrane emulsification with polymerization and solvent evaporation method was tested. Technically it showed to be a more complex approach than nano-emulsion.

With membrane emulsification using both PCL and polystyrene system it was not possible to achieve the critical pressure needed to obtain an emulsion with a hydrophilic membrane of 0.4µm. This limits the size of the final beads produced. In the PCL system a 7% solution of PCL in chloroform has to be used in order to have a not so viscous solution that is possible to emulsify. It was also difficult to incorporate the iron oxide in the final product. It was possible to do so with PCL, where 2.84% of iron oxide was incorporated using a 0.8µm hydrophilic membrane.

The best results with membrane emulsification and polymerization with solvent evaporation were obtained with the polystyrene system using a 0.8µm hydrophilic membrane where a low polydispersity index of 0.19 was obtained and a mean size of 500nm. However this result did not comprise iron oxide, therefore the final product is not magnetic. There was not substantial difference found between DCM and hexane in the polystyrene system.

Regarding the optimization of the magnetoresistive platform, the COMSOL multiphysics model was adequate. The different simulations that were performed matched the actual readings. There is however a need to take in consideration that the magnet that was read was not totally homogeneous and several high intensity spots were shown. Other noticeable difference was the negative values that show outside the magnet dimensions in the simulated planes. This was due the to the fact that in the simulated planes there is a necessity to simulate an air box were the magnetic field is comprised and therefore simulated, where in the reading planes this air box is infinite therefore there is no confinement to the magnetic field.

Since the model was robust enough, it was possible to address the initial problem of the magnet dimensions. A minimum of approximately $Hz = 1000\ Oe$ and a maximum available area with minimized Hx ($|Hx|$< 10 Oe) component.

This conditions are required for a suitable magnetization of the beads in z direction thus ensuring a larger transduced signal by the magnetoresistive sensors. Secondly a minimized Hx is required to prevent saturation of the sensor linear range response. Suitable magnet dimensions were 30x30x3 mm.

As future work it is important to optimize the membrane emulsification with solvent evaporation method. This could be tackled in various ways. A possible approach is to do a systematic study with different pore size membranes. The polystyrene formulation comprising iron oxide should be employed in the system using different membrane pore sizes in order to be able to study the variation of sizes of the final product and the relationships in critical pressures. This is important given the difficulty in knowing the size that is going to be obtained after the solvent has evaporated. The same approach can and should be done with the 7% PCL system with iron oxide in order to be able to decrease the mean average size of the final product. The membrane emulsification with solvent evaporation method even though it is technically more challenging should be preferred, since it will address the main problem of the nano-emulsion the polidispersity of the final product inherent to the technique.

Concerning the COMSOL multiphysics model used to optimize the magnetoresistive platform, it can be improved. This should be done with the addition of microfluidic simulations to the model. With this upgrade it should be possible to study the nanocomposite magnetic beads behavior when a magnetic field is present. This improvement will aid in the comprehension of the nanocomposite beads in a microfluidic flow with different velocities while in a magnetic field. It is a robust manner to increase the efficiency of the platform.

A complete different application where work could be conducted using the nanocomposite magnetic beads, is using them as MRI contrast agents. In this case it will be necessary to perform a study of the nanocomposite magnetic beads with the same size and different iron oxide contents or different sizes and the same iron oxide content, in order to access through relaxometry how it affects T1 and T2 relaxation times. This is important to understand if the polymer matrix of the nanocomposite affects the relaxation times and in what way.

Nanocomposite polymer beads are very versatile and the fact that the formulations of the organic phase can be changed indicates a broad range of different applications, other than cell detection where they could be of purpose.

Bibliography

[1] M. Balic, H. Lin, and A. Williams, “Progress in circulating tumor cell capture and analysis: implications for cancer management,” *Expert Rev Mol Diagn*, vol. 12, no. 3, pp. 303–312, 2012.

[2] M. C. Miller, G. V Doyle, and L. W. M. M. Terstappen, “Significance of Circulating Tumor Cells Detected by the CellSearch System in Patients with Metastatic Breast Colorectal and Prostate Cancer.,” *J. Oncol.*, vol. 2010, p. 617421, 2010.

[3] A. M. C. Barradas and L. W. M. M. Terstappen, “Towards the Biological Understanding of CTC: Capture Technologies, Definitions and Potential to Create Metastasis.,” *Cancers (Basel).*, vol. 5, no. 4, pp. 1619–42, Jan. 2013.

[4] K. F. Ho, N. E. Gouw, and Z. Gao, “Quantification techniques for circulating tumor cells,” *Trends Anal. Chem.*, vol. 64, pp. 173–182, 2015.

[5] J. Loureiro, R. Ferreira, S. Cardoso, P. P. Freitas, J. Germano, C. Fermon, G. Arrias, M. Pannetier-Lecoeur, F. Rivadulla, and J. Rivas, “Toward a magnetoresistive chip cytometer: Integrated detection of magnetic beads flowing at cm/s velocities in microfluidic channels,” *Appl. Phys. Lett.*, vol. 95, pp. 1–4, 2009.

[6] V. C. Martins, J. Germano, F. a. Cardoso, J. Loureiro, S. Cardoso, L. Sousa, M. Piedade, L. P. Fonseca, and P. P. Freitas, “Challenges and trends in the development of a magnetoresistive biochip portable platform,” *J. Magn. Magn. Mater.*, vol. 322, pp. 1655–1663, 2010.

[7] A. Vila, V. C. Martins, A. Chícharo, C. Rodriguez-abreu, A. C. Fernandes, F. A. Cardoso, S. Cardoso, J. Rivas, and P. Freitas, “Customized Design of Magnetic Beads for Dynamic Magnetoresistive Cytometry,” vol. 50, no. 11, pp. 18–21, 2014.

[8] T. R. Ashworth, “A case of cancer in which cells similar to those in the tumours were seen in the blood after death,” *Aust Med J*, vol. 14, no. 3, pp. 146–149, 1869.

[9] M. Balic, A. Williams, H. Lin, R. Datar, and R. J. Cote, “Circulating tumor cells: from bench to bedside.,” *Annu. Rev. Med.*, vol. 64, pp. 31–44, Jan. 2013.

[10] M. Cristofanilli, G. T. Budd, M. J. Ellis, A. Stopeck, J. Matera, M. C. Miller, J. M. Reuben, G. V Doyle, W. J. Allard, L. W. M. M. Terstappen, and D. F. Hayes, “Circulating tumor cells, disease progression, and survival in metastatic breast cancer.,” *N. Engl. J. Med.*, vol. 351, pp. 781–791, 2004.

[11] G. Vona, a Sabile, M. Louha, V. Sitruk, S. Romana, K. Schütze, F. Capron, D. Franco, M. Pazzagli, M. Vekemans, B. Lacour, C. Bréchot, and P. Paterlini-Bréchot, “Isolation by size of epithelial tumor cells : a new method for the immunomorphological and molecular

characterization of circulatingtumor cells.," *Am. J. Pathol.*, vol. 156, no. 1, pp. 57–63, 2000.

[12] H. Markides, M. Rotherham, and a. J. El Haj, "Biocompatibility and toxicity of magnetic nanoparticles in regenerative medicine," *J. Nanomater.*, vol. 2012, pp. 13–15, 2012.

[13] U. Schwertmann and R. M. Cornell, "Magnetite," in *Iron Oxides in the Laboratory*, Wiley-VCH Verlag GmbH, 2007, pp. 135–140.

[14] A. K. Gupta and M. Gupta, "Synthesis and surface engineering of iron oxide nanoparticles for biomedical applications.," *Biomaterials*, vol. 26, no. 18, pp. 3995–4021, Jun. 2005.

[15] G. F. Goya, T. S. Berquó, F. C. Fonseca, and M. P. Morales, "Static and dynamic magnetic properties of spherical magnetite nanoparticles," *J. Appl. Phys.*, vol. 94, no. 2003, pp. 3520–3528, 2003.

[16] C. Liu and Z. J. Zhang, "Size-Dependent Superparamagnetic Properties of Mn Spinel Ferrite Nanoparticles Synthesized from Reverse Micelles," *Chem. Mater.*, vol. 13, no. 6, pp. 2092–2096, Jun. 2001.

[17] M. a. Willard, L. K. Kurihara, E. E. Carpenter, S. Calvin, and V. G. Harris, "Chemically prepared magnetic nanoparticles," *Int. Mater. Rev.*, vol. 49, no. 3, pp. 125–170, 2004.

[18] N. a Frey, S. Peng, K. Cheng, and S. Sun, "Magnetic nanoparticles: synthesis, functionalization, and applications in bioimaging and magnetic energy storage.," *Chem. Soc. Rev.*, vol. 38, no. May, pp. 2532–2542, 2009.

[19] C. E. Sjøgren, K. Briley-Sæbø, M. Hanson, and C. Johansson, "Magnetic characterization of iron oxides for magnetic resonance imaging," *Magn. Reson. Med.*, vol. 31, no. 3, pp. 268–272, 1994.

[20] G. W. Reimers and S. E. Khalafalla, *Preparing Magnetic Fluids by a Peptizing Method*. Bureau of Mines, U.S. Department of the Interior, 1972.

[21] D. K. Kim, Y. Zhang, W. Voit, K. V. Rao, and M. Muhammed, "Synthesis and characterization of surfactant-coated superparamagnetic monodispersed iron oxide nanoparticles," *J. Magn. Magn. Mater.*, vol. 225, pp. 30–36, 2001.

[22] M. Bowker, "Surface science: The going rate for catalysts," *Nat Mater*, vol. 1, no. 4, pp. 205–206, Dec. 2002.

[23] P. Becher, *Emulsions: theory and practice*. Chemical Rubber Co. Scientific Review Press.; Cleveland. Ohio. USA 2nd ed., 1965.

[24] C. Rodríguez-Abreu and A. Vila, "Nano-droplet systems by surfactant self-assembly and applications in the pharmaceutical industry," *Curr. Top. Med. Chem.*, vol. 14, no. 6, pp. 747–765, 2014.

[25] T. G. Mason, S. M. Graves, J. N. Wilking, and M. Y. Lin, “Extreme emulsification: Formation and structure of nanoemulsions,” *Condens. Matter Phys.*, vol. 9, no. 1, pp. 193–199, 2006.

[26] a. Maali and M. T. H. Mosavian, “Preparation and Application of Nanoemulsions in the Last Decade (2000–2010),” *J. Dispers. Sci. Technol.*, vol. 34, no. December 2012, pp. 92–105, 2013.

[27] N. Anton, J. P. Benoit, and P. Saulnier, “Design and production of nanoparticles formulated from nano-emulsion templates-A review,” *J. Control. Release*, vol. 128, pp. 185–199, 2008.

[28] H. Chen, C. Khemtong, X. Yang, X. Chang, and J. Gao, “Nanonization strategies for poorly water-soluble drugs,” *Drug Discov. Today*, vol. 16, no. 7–8, pp. 354–360, 2011.

[29] M. M. Fryd and T. G. Mason, “Advanced Nanoemulsions,” *Annu. Rev. Phys. Chem.*, vol. 63, pp. 493–518, 2012.

[30] W. Bonrath and R. a. P. Schmidt, “Ultrasound in Synthetic Organic Chemistry,” *Adv. Org. Synth.*, vol. 1, pp. 81–117, 2005.

[31] W. Jackson, B. Y. C. Bondy, and K. Sollner, “On the Mechanism of Emulsification by Ultrasonic Waves,” 1935.

[32] M. Ashokkumar, “The characterization of acoustic cavitation bubbles - An overview,” *Ultrason. Sonochem.*, vol. 18, no. 4, pp. 864–872, 2011.

[33] E. Nazarzadeh and S. Sajjadi, “Viscosity effects in miniemulsification via ultrasound,” *AIChE J.*, vol. 56, no. 10, pp. 2751–2755, 2010.

[34] S. Abbas, K. Hayat, E. Karangwa, M. Bashari, and X. Zhang, “An Overview of Ultrasound-Assisted Food-Grade Nanoemulsions,” *Food Eng. Rev.*, vol. 5, pp. 139–157, 2013.

[35] P. Taylor and R. H. Ottewill, “Ostwald Ripening in O/W Miniemulsions formed by the Dilution of O/W Microemulsions,” *Prog. Colloid Polym. Sci.*, vol. 97, pp. 199–203, 1994.

[36] P. Taylor, “Ostwald ripening in emulsions,” *Adv. Colloid Interface Sci.*, vol. 75, pp. 107–163, 1998.

[37] T. Delmas, H. Piraux, A. C. Couffin, I. Texier, F. Vinet, P. Poulin, M. E. Cates, and J. Bibette, “How to prepare and stabilize very small nanoemulsions,” *Langmuir*, vol. 27, no. 16, pp. 1683–1692, 2011.

[38] E. F. Craparo, G. Cavallaro, M. L. Bondì, D. Mandracchia, and G. Giammona, “PEGylated Nanoparticles based on a polyaspartamide. preparation, physico-chemical characterization, and intracellular uptake,” *Biomacromolecules*, vol. 7, no. 11, pp. 3083–3092, 2006.

[39] M. A. Bradley, S. W. Prescott, H. A. S. Schoonbrood, K. Landfester, and F. Grieser, “Miniemulsion copolymerization of methyl methacrylate and butyl acrylate by ultrasonic initiation,” *Macromolecules*, vol. 38, no. 15, pp. 6346–6351, 2005.

[40] M. Antonietti, “Polyreactions in miniemulsions,” *Prog. Polym. Sci.*, vol. 27, no. 4, pp. 689–757, May 2002.

[41] K. Landfester, N. Bechthold, F. Tiarks, and M. Antonietti, “Formulation and stability mechanisms of polymerizable miniemulsions,” *Macromolecules*, vol. 32, no. 16, pp. 5222–5228, 1999.

[42] S. M. Joscelyne and G. Trägårdh, “Membrane emulsification - A literature review,” *J. Memb. Sci.*, vol. 169, no. April 1999, pp. 107–117, 2000.

[43] V. Schröder, O. Behrend, and H. Schubert, “Effect of Dynamic Interfacial Tension on the Emulsification Process Using Microporous, Ceramic Membranes,” *J. Colloid Interface Sci.*, vol. 202, no. 202, pp. 334–340, 1998.

[44] R. a. Williams, S. J. Peng, D. a. Wheeler, N. C. Morley, D. Taylor, M. Whalley, and D. W. Houldsworth, “Controlled Production of Emulsions Using a Crossflow Membrane,” *Chem. Eng. Res. Des.*, vol. 76, no. June 1997, pp. 902–910, 1998.

[45] J. Loureiro, C. Fermon, M. Pannetier-Lecoeur, G. Arrias, R. Ferreira, S. Cardoso, and P. P. Freitas, “Magnetoresistive detection of magnetic beads flowing at high speed in microfluidic channels,” *IEEE Trans. Magn.*, vol. 45, no. NOVEMBER, pp. 4873–4876, 2009.

[46] A. Fernandes, C. Duarte, F. Cardoso, R. Bexiga, S. Cardoso, and P. Freitas, “Lab-on-Chip Cytometry Based on Magnetoresistive Sensors for Bacteria Detection in Milk,” *Sensors*, vol. 14, pp. 15496–15524, 2014.

[47] C. A Pecharromán, T. A González-Carreño, and A. Iglesias, “The infrared dielectric properties of maghemite, γ-Fe2O3, from reflectance measurement on pressed powders,” *J Phys. Chem. Miner.*, vol. 22, pp. 21–29, 1995.

[48] W. Kim, C.-Y. Suh, S.-W. Cho, K.-M. Roh, H. Kwon, K. Song, and I.-J. Shon, “A new method for the identification and quantification of magnetite-maghemite mixture using conventional X-ray diffraction technique.,” *Talanta*, vol. 94, pp. 348–52, May 2012.

[49] N. Tran, A. Mir, D. Mallik, A. Sinha, S. Nayar, and T. J. Webster, “Bactericidal effect of iron oxide nanoparticles on Staphylococcus aureus,” *Int. J. Nanomedicine*, vol. 5, pp. 277–283, 2010.

[50] T. Ungár, “Microstructural parameters from X-ray diffraction peak broadening,” *Scr. Mater.*, vol. 51, no. 8, pp. 777–781, 2004.

[51] G. D. Chanana and B. B. Sheth, “Particle size reduction of emulsions by formulation design-II: effect of oil and surfactant concentration.,” *PDA J. Pharm. Sci. Technol.*, vol. 49, no. 2, pp. 71–76, 1995.

[52] T. Tadros, P. Izquierdo, J. Esquena, and C. Solans, “Formation and stability of nano-emulsions,” *Adv. Colloid Interface Sci.*, vol. 108–109, pp. 303–318, 2004.

Appendix

Table 14- Comparison of 0.1 mm planes, read and simulated (units Oe)

Plane	Simulation	Reading
0.1mm	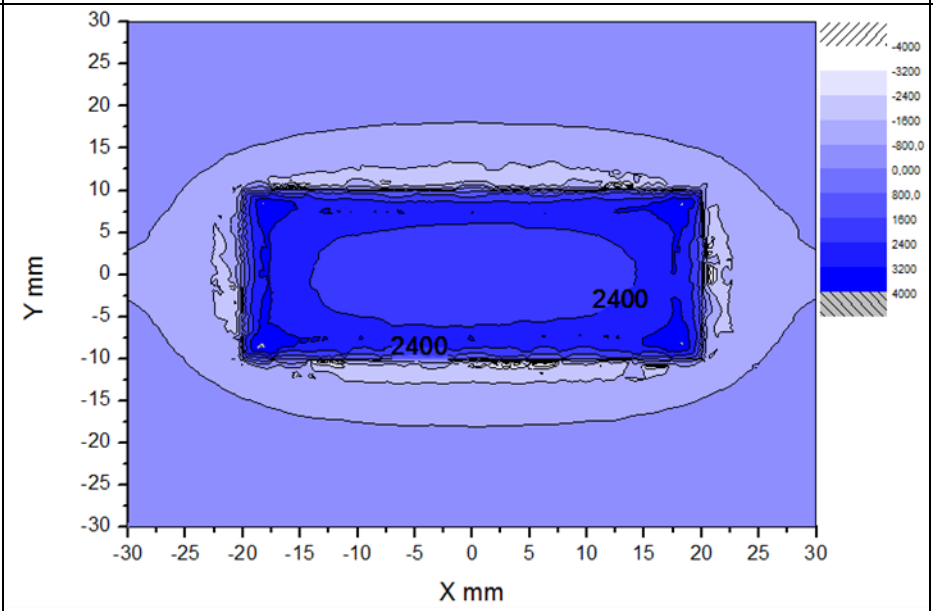	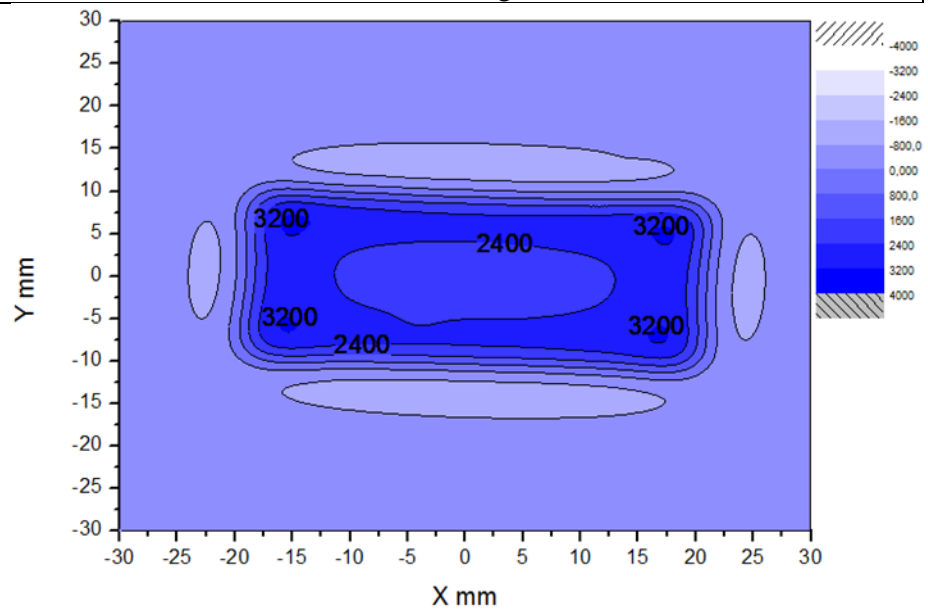

Table 15- Comparison of 1.1 mm planes, read and simulated (units Oe)

Plane	Simulation	Reading
1.1mm	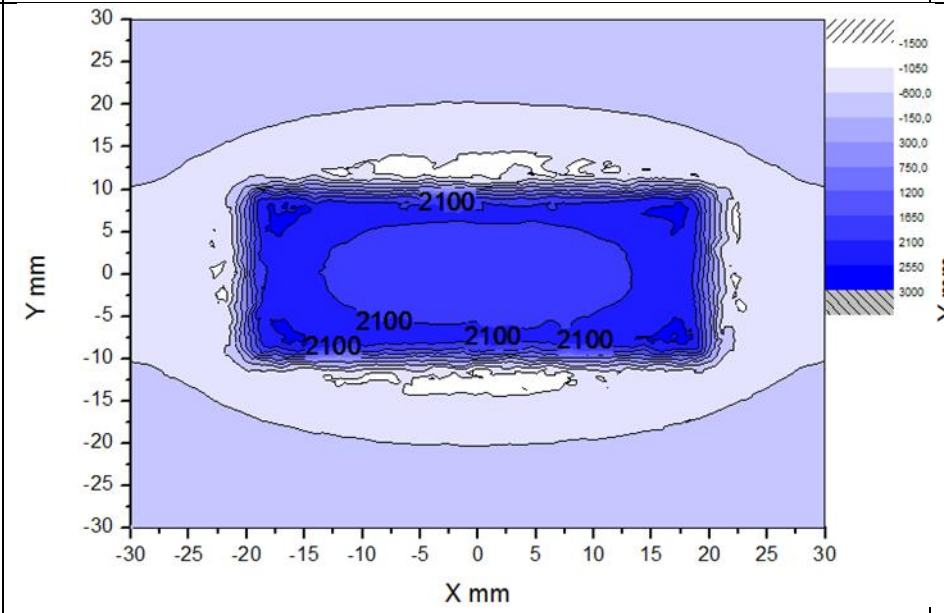	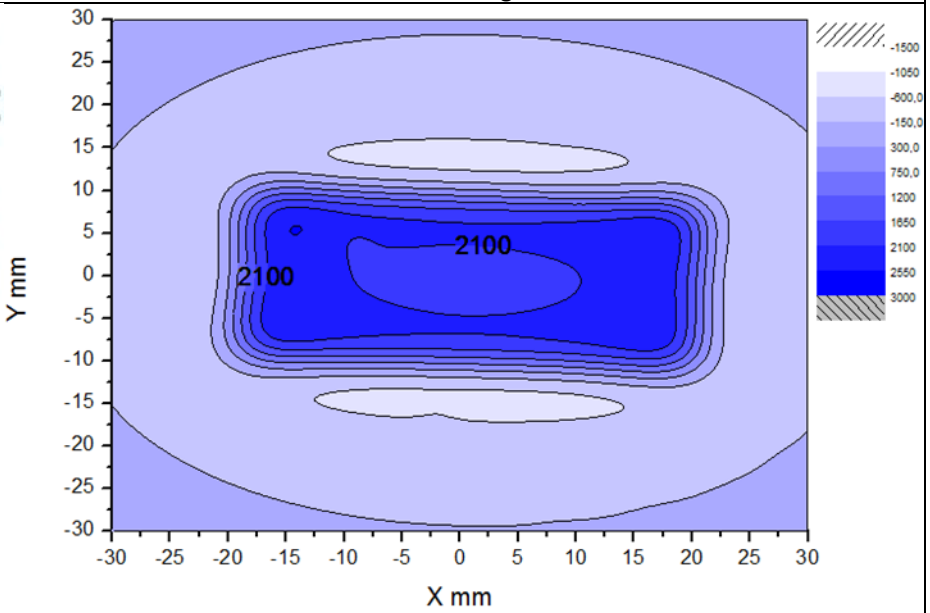

Table 16- Comparison of 2.1 mm planes, read and simulated (units Oe)

Plane	Simulation	Reading
2.1mm	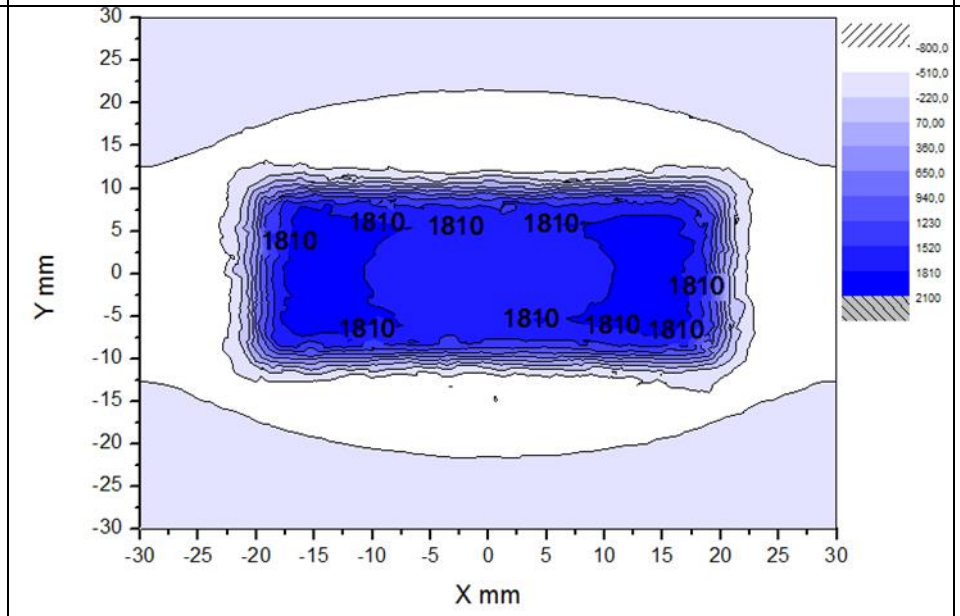	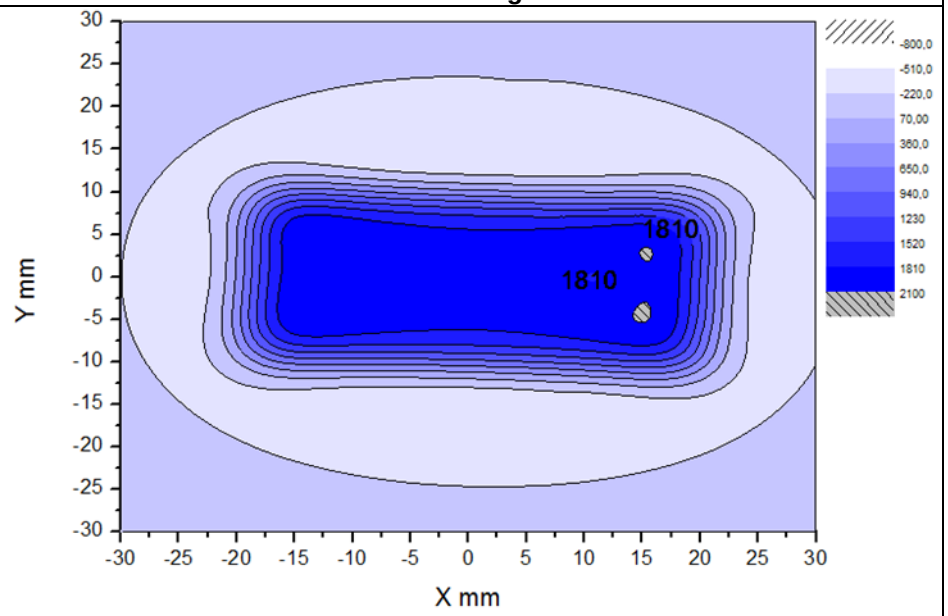

Table 17- Comparison of 3.1 mm planes, read and simulated (units Oe)

Plane	Simulation	Reading
3.1mm	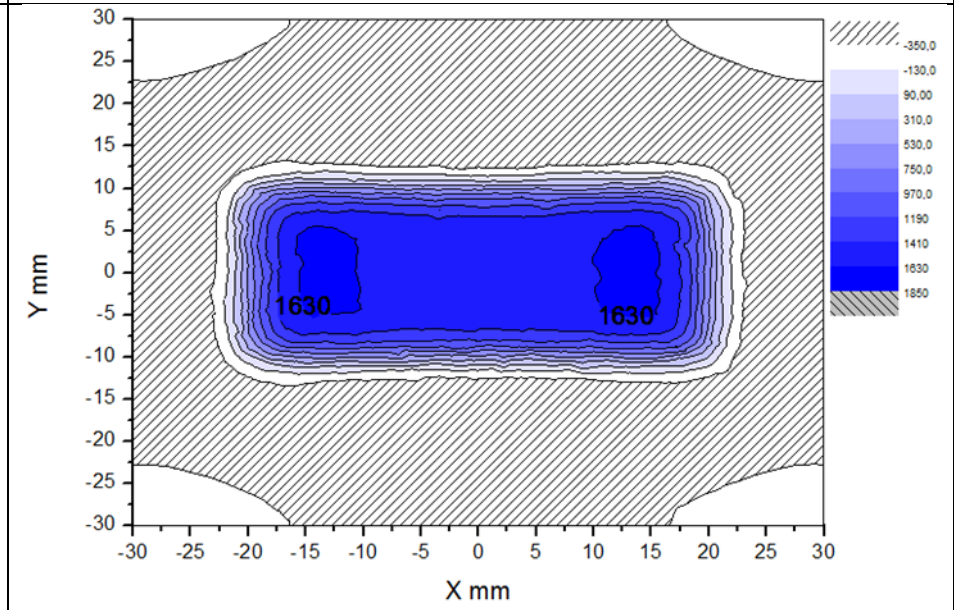	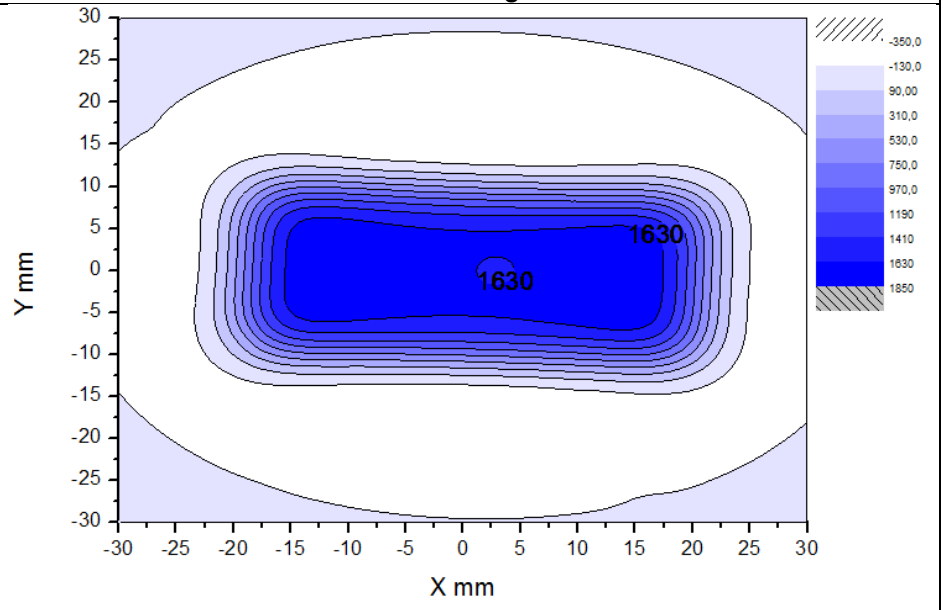

Table 18- Comparison of 4.1 mm planes, read and simulated (units Oe)

Plane	Simulation	Reading
4.1mm	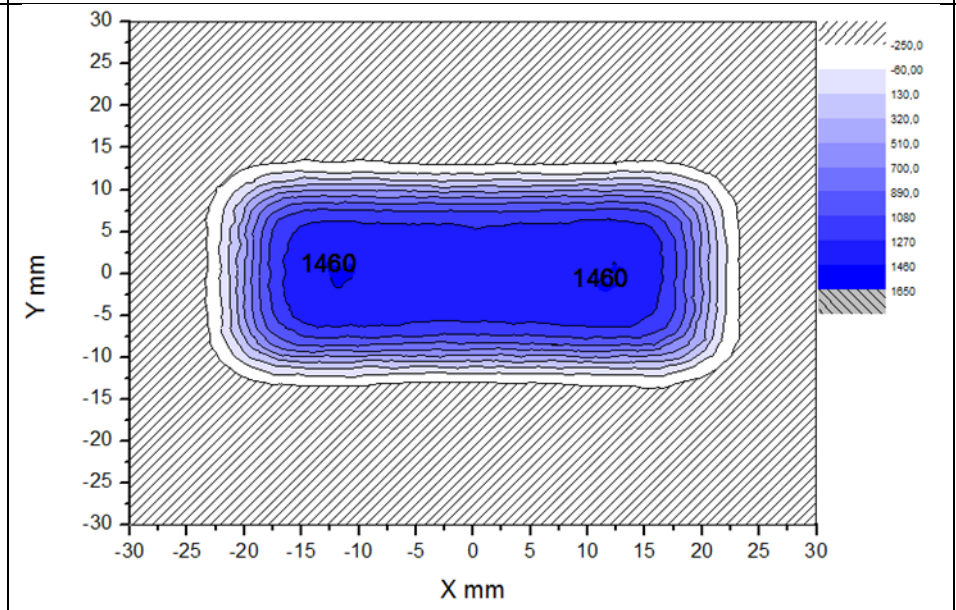	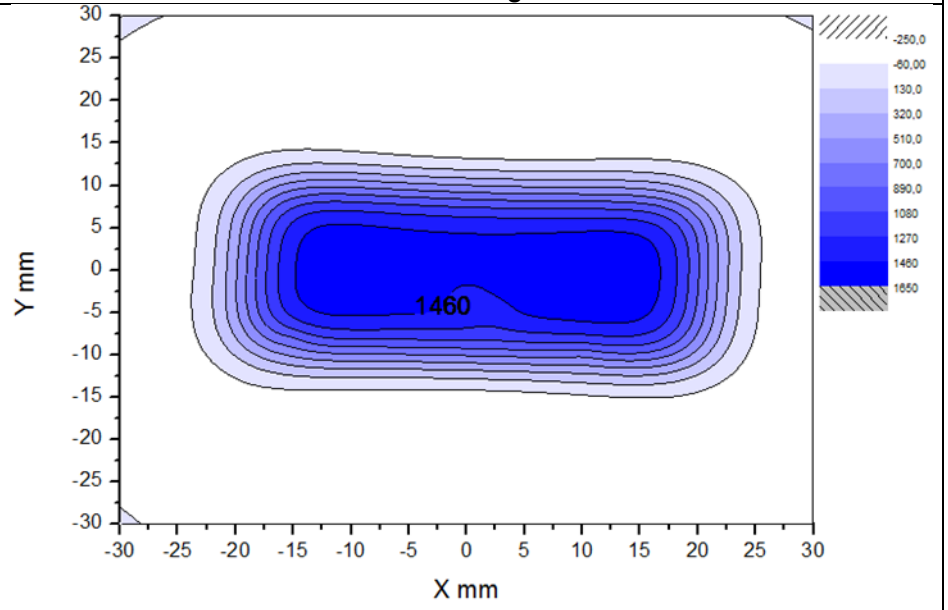

Table 19- Comparison of 5.1 mm planes, read and simulated (units Oe)

Plane	Simulation	Reading
5.1mm	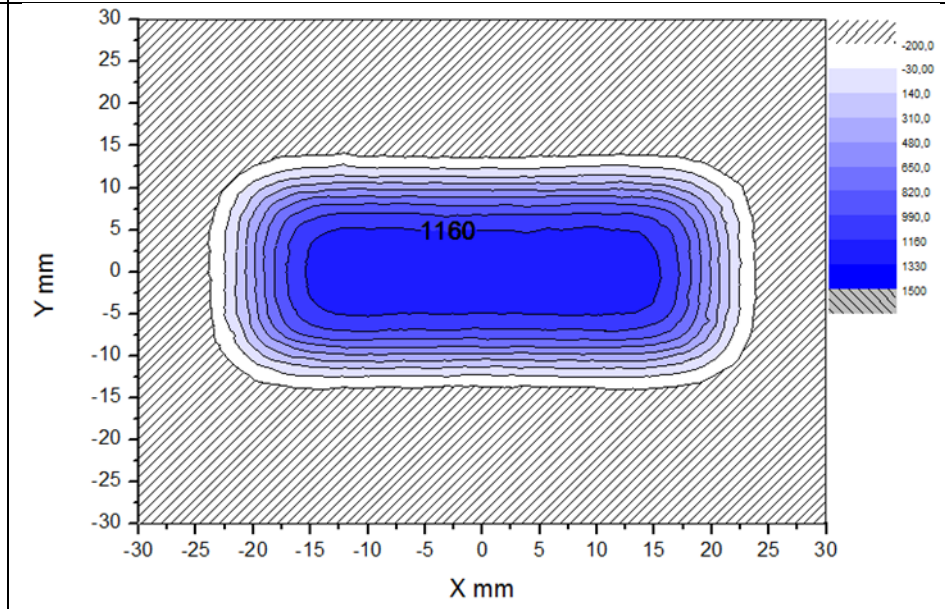	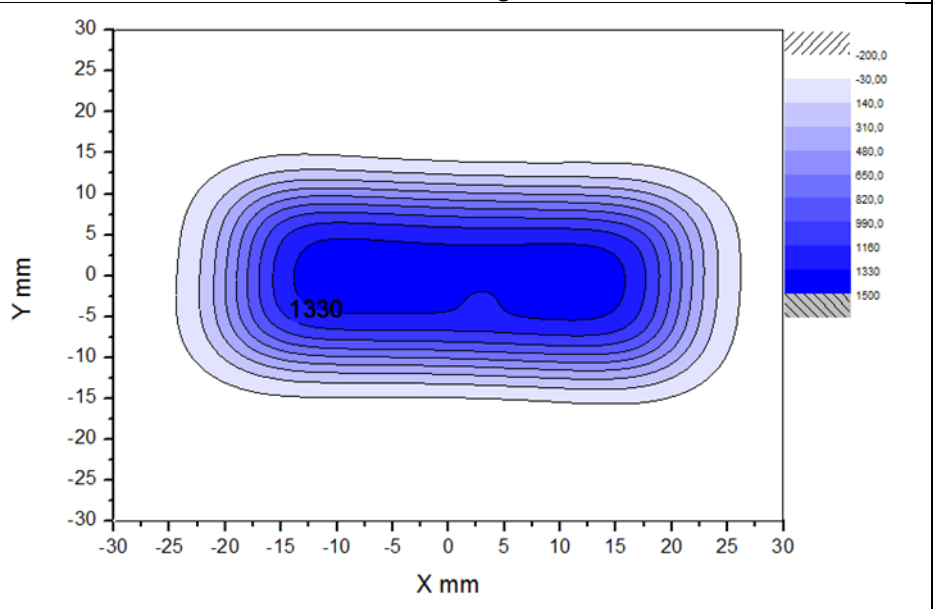

Table 20- Comparison of 6.1 mm planes, read and simulated (units Oe)

Plane	Simulation	Reading
6.1mm	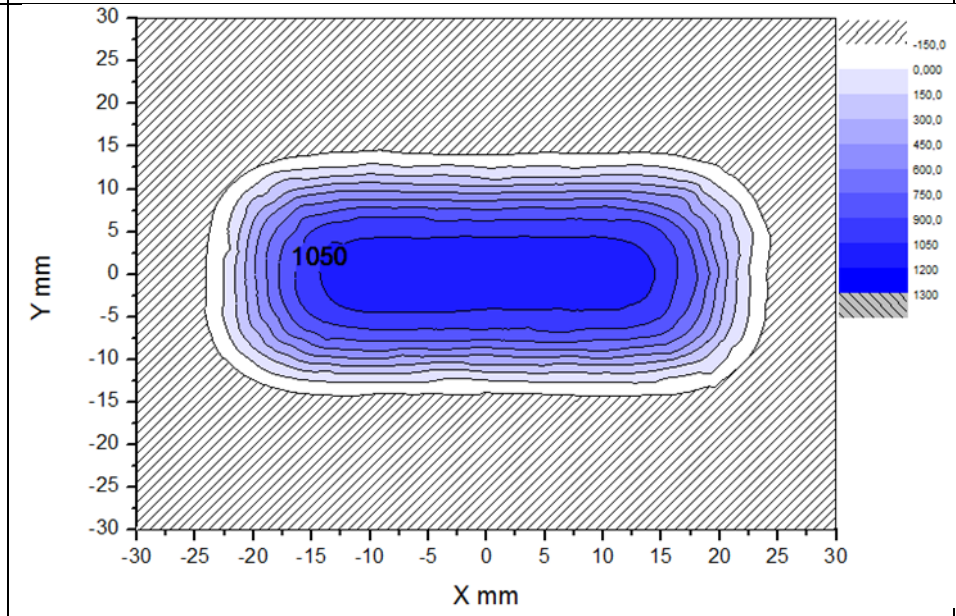	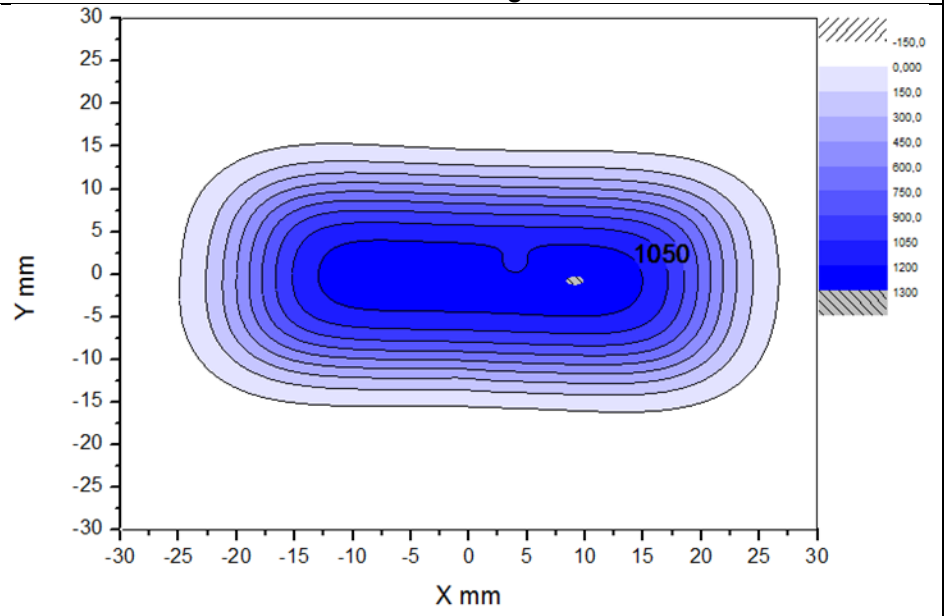

Table 21 Comparison of 7.1 mm planes, read and simulated (units Oe)

Plane	Simulation	Reading
7.1mm	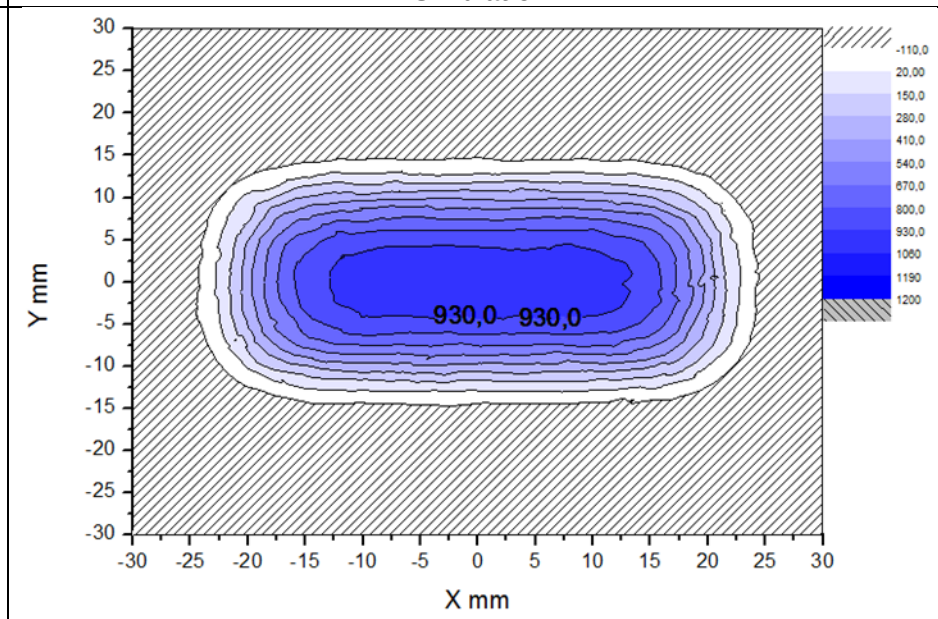	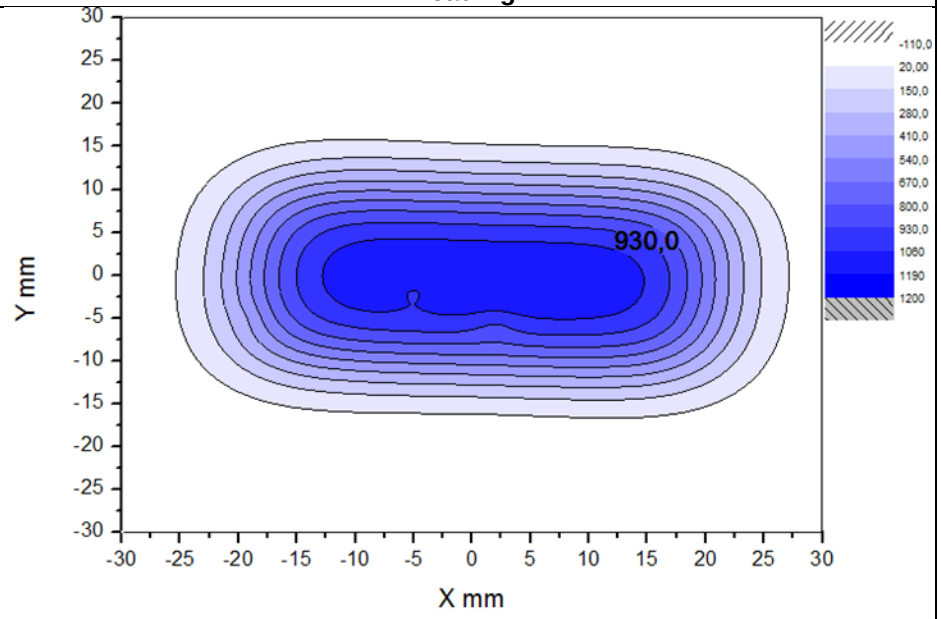

Table 22- Comparison of 8.1 mm planes, read and simulated (units Oe)

Plane	Simulation	Reading
8.1mm	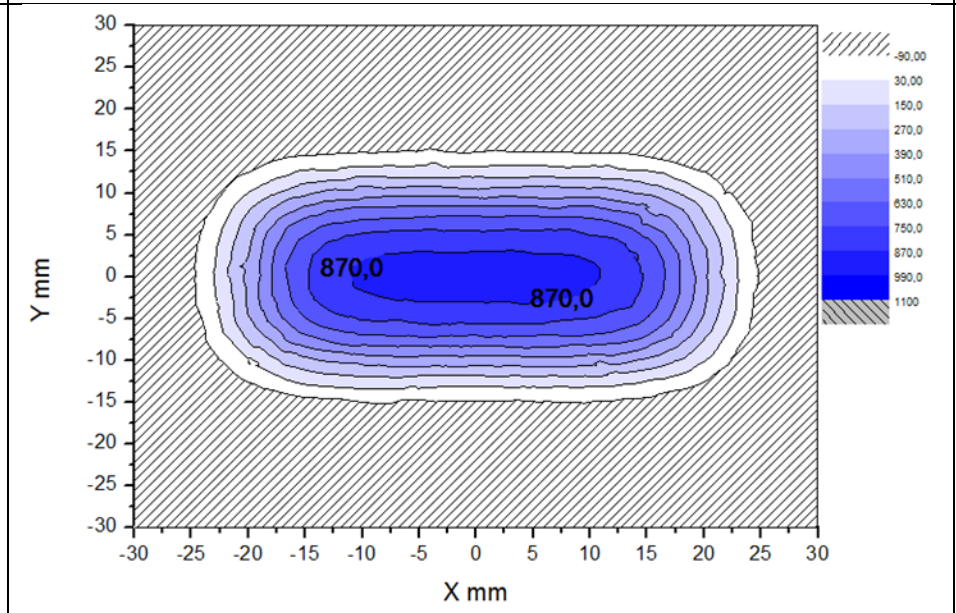	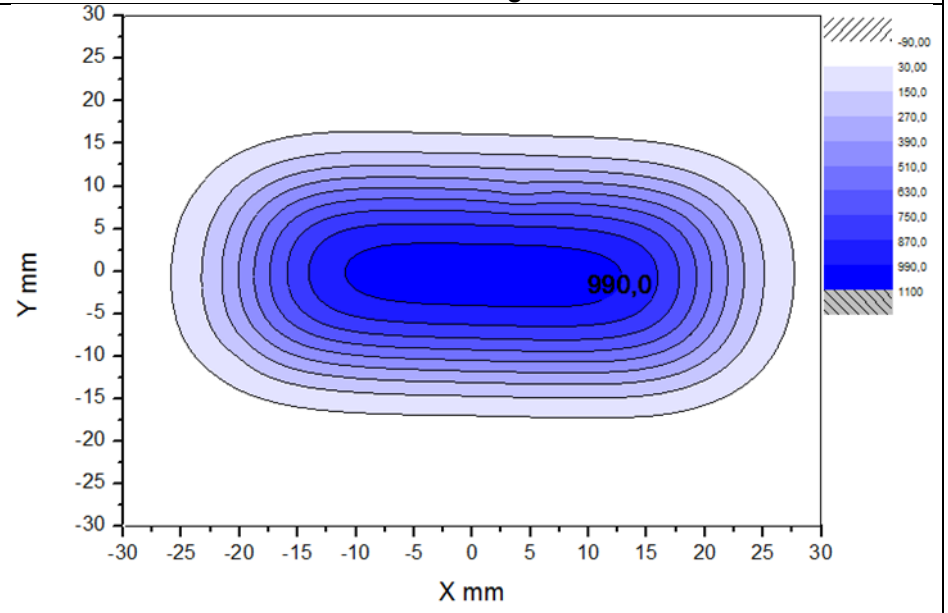

Table 23- Comparison of 9.1 mm planes, read and simulated (units Oe)

Plane	Simulation	Reading
9.1mm	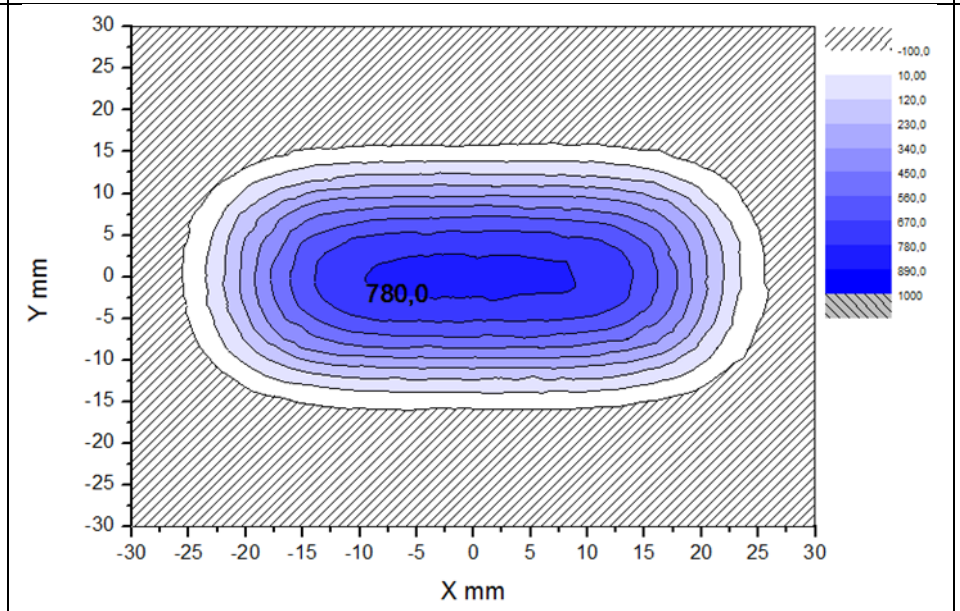	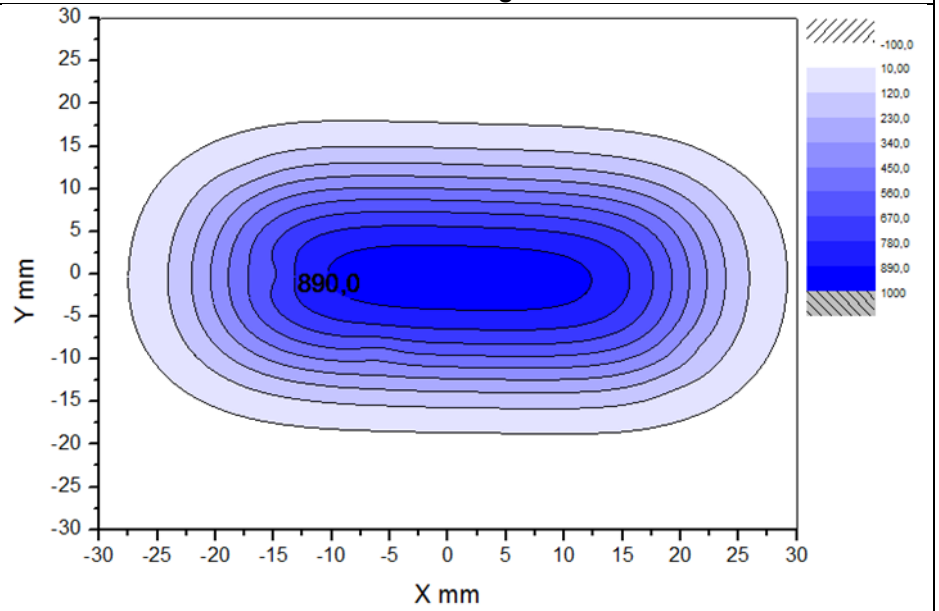

Table 24- Comparison of 10.1 mm planes, read and simulated (units Oe)

Plane	Simulation	Reading
10.1 mm